

Supporting information

Nucleic Acid-Binding Bis-Acridine Orange Dyes with Improved Properties for Bioimaging and PCR Applications

Olesia Kulyk¹, Rostyslav Svoiakov¹, Olga Kolosova¹, Ivanna Prylutska², Tudor Vasiliu^{3,4}, Razvan Puf³, Francesca Mocchi⁵, Aatto Laaksonen^{3,6,7,8}, Sergiy Perepelytsya⁹, Alexander Krivoshey¹, Dmytro Kobzev^{1,10}, Zenoviy Tkachuk² and Anatoliy Tatarets^{1,*}

¹ Institute of Functional Materials Chemistry of State Scientific Institution "Institute for Single Crystals" of National Academy of Sciences of Ukraine, Kharkiv, 61072, Ukraine

² Institute of Molecular Biology and Genetics of the National Academy of Sciences of Ukraine, Kyiv, 03143, Ukraine

³ Center of Advanced Research in Bionanoconjugates and Biopolymers, "Petru Poni" Institute of Macromolecular Chemistry, Iasi, 700487, Romania

⁴ The Research Institute of the University of Bucharest (ICUB), Bucharest, 050663, Romania

⁵ Dipartimento di Scienze Chimiche e Geologiche, Università di Cagliari, Cagliari, 09042, Italy

⁶ Department of Materials and Environmental Chemistry, Division of Physical Chemistry, Arrhenius Laboratory, Stockholm University, Stockholm, 106 91, Sweden

⁷ State Key Laboratory of Materials-Oriented and Chemical Engineering, Nanjing Tech University, Nanjing, 210009, PR China

⁸ Department of Engineering Sciences and Mathematics, Division of Energy Science, Luleå University of Technology, Luleå, 97187, Sweden

⁹ Bogolyubov Institute for Theoretical Physics of the National Academy of Science of Ukraine, Kyiv, 03143, Ukraine

¹⁰ Institute for Experimental Molecular Imaging, Center for Biohybrid Medical Systems, RWTH Aachen University Clinic, Aachen, 52074, Germany

* Dr. Anatoliy Tatarets, Email: tatarets@isc.kh.ua

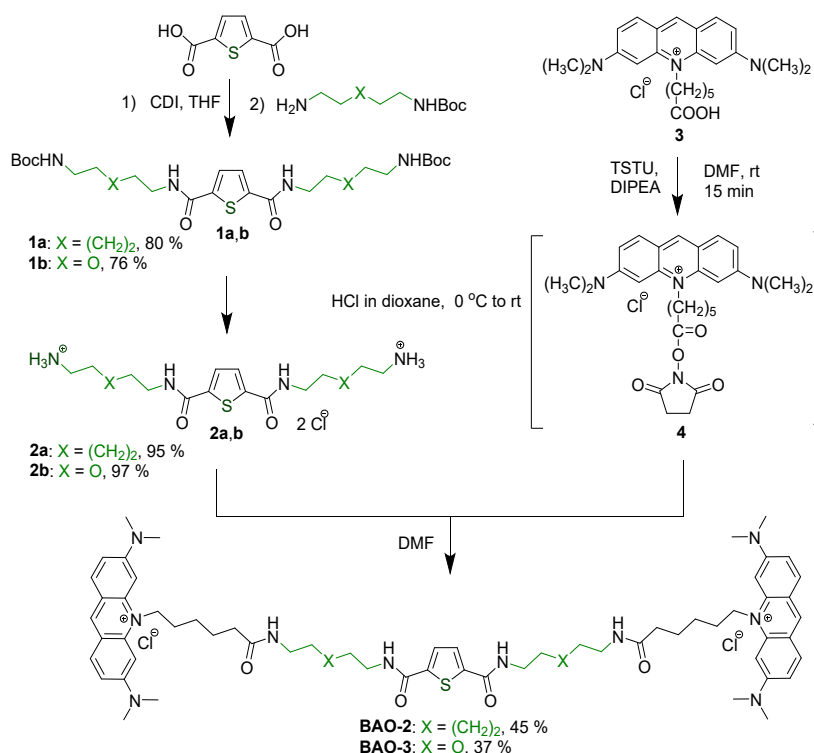
Institute of Functional Materials Chemistry of State Scientific Institution "Institute for Single Crystals" of National Academy of Sciences of Ukraine, 60 Nauky Ave., 61072 Kharkiv, Ukraine.

Table of contents

S1. Synthesis of BAO dyes	S3
S1.1. Materials and methods.....	S3
S1.2. Synthetic procedures.....	S5
S2. Spectral measurements	S8
S2.1. Absorption, fluorescence excitation and emission spectra	S8
S2.2. Fluorescence lifetimes	S9
S2.3. Binding constants	S12
S2.4. Brightness and stability tests	S13
S3. Cell imaging	S16
S3.1. Cytotoxicity assay	S16
S3.2. Results of confocal laser scanning microscopy.....	S17
S4. qPCR experiments	S19
S5. MD simulations	S23
S6. ¹ H NMR spectra of the obtained compounds	S29
S7. ¹³ C NMR spectra of the obtained compounds	S32
S8. HRMS spectra of the BAO dyes	S35
References	S38

S1. Synthesis of BAO dyes

New dimeric dyes **BAO-2** and **BAO-3** were synthesized similarly to our previously reported procedure,¹ as shown in [Scheme 1](#). The diaminium salts **2a** and **2b** were obtained by reaction of corresponding monoprotected diamines with thiophene-2,5-dicarboxylic acid in the presence of 1,1'-carbonyldiimidazole (CDI) followed by the cleavage of Boc-protecting groups with 25 wt. % solution of HCl in dioxane. The acridine orange derivative **3** quaternized with 6-bromohexanoic acid was activated with *N,N,N',N'*-tetramethyl-*O*-(*N*-succinimidyl)uronium tetrafluoroborate (TSTU) to yield *N*-hydroxysuccinimide ester (NHS-ester) **4**.² The *in situ* generated NHS-ester was then reacted with the diaminium salt **2a** or **2b** in DMF in the presence of DIPEA to give target dimeric dyes **BAO-2** and **BAO-3** in 45 % and 37 % yields, respectively.



Supplementary Scheme S1. Synthesis of dimeric dyes **BAO-2** and **BAO-3**.

S1.1. Materials and methods

Starting materials for the synthesis of the cited compounds, 2,5-thiophenedicarboxylic acid was purchased from *Matrix Scientific*, *tert*-butyl (2-(2-aminoethoxy)ethyl)carbamate and *tert*-butyl (6-aminohexyl)carbamate hydrochloride were from *UOSlab*, *N,N,N',N'*-tetramethyl-

O-(*N*-succinimidyl)uronium tetrafluoroborate (TSTU), DNA (low molecular weight from salmon sperm) and 1,1'-carbonyldiimidazole (CDI) were from *Sigma-Aldrich*. **EG** was purchased from *Biotium*. *N,N*-Dimethylformamide (DMF) and tetrahydrofuran (THF) were dried by known methods and distilled immediately before use. All other reagents were commercially available and used without further purification, unless otherwise stated. Dimeric dye **BAO-1** was synthesized according to our previously reported protocol.¹

Tris buffer pH 8.0 (10 mM) was prepared by dissolving *tris*(hydroxymethyl)-aminomethane hydrochloride (Trizma[®] hydrochloride (Sigma-Aldrich), 1.57 g) in 0.5 L Milli-Q water and the pH was adjusted to 8.0 with solution of NaOH. The pH value was controlled with pH-meter *Hanna Instruments pH 213*. The resulting solution was adjusted to 1 L with Milli-Q water.

Thin layer chromatography (TLC) was conducted on pre-coated plates (*Merck Silica gel 60 F254* or *Merck Silica gel 60 RP-18 F254*) with visualization by fluorescent indicator UV254 using CHCl₃/methanol or CH₃CN/water mixtures, respectively, as eluents.

Column chromatography was performed with Al₂O₃ (*Merck Aluminium oxide 90 active neutral, 70–230 mesh ASTM*), silica gel (*Merck Silica gel 60, 70–230 mesh ASTM*) or reversed phase silica gel (*Merck Silica gel 60 RP-18, 40–63 μm*).

HPLC analyses were performed on a *Bischoff* module chromatograph equipped with a column Nucleosil 100-5-C18 (4.0×150 mm, 5 μm; acetonitrile or azeotropic mixture of acetonitrile and water (14.0–17.2 wt. % water, bp 76.0–76.2 °C) served as eluents), or *Agilent 1100* module chromatograph equipped with LC column Luna Omega 5 μm C18 100 Å (4.6×250 mm; mixtures of acetonitrile, water and H₃PO₄ (0.05% v/v) served as eluents), elution was implemented by the gradient scheme from 10% to 90% v/v of acetonitrile in the mixture.

¹H NMR and ¹³C NMR spectra were registered in DMSO-*d*₆ using a *Varian MR-400* spectrometer or a *Bruker Avance III HD* spectrometer at room temperature (400 MHz and 101 MHz for ¹H and ¹³C, respectively). Chemical shifts were reported in ppm using the solvent residual signal as an internal reference ($\delta_{\text{H}}(\text{DMSO-}d_6) = 2.50 \text{ ppm}$, $\delta_{\text{C}}(\text{DMSO-}d_6) = 39.52 \text{ ppm}$).³

Melting points were measured using a *Köfler* hot bench apparatus.

Mass spectra were collected using a mass spectrometer *Waters Micromass Quattro Micro API*.

The C, H, N elemental analysis was performed by a *EuroVector Euro EA 3000 EA-IRMS* elemental analyzer.

HRMS spectra were measured using ThermoFisher Scientific LTQ-Orbitrap XL.

S1.2. Synthetic procedures

Di-*tert*-butyl (((thiophene-2,5-dicarbonyl)bis(azanediyl))bis(hexane-6,1-diyl)) dicarbamate (1a) (80%) was obtained according to our previously reported protocol.¹ Recrystallized from acetonitrile/dioxane, 2:1 (v/v). White solid, m.p. 171–173 °C (from acetonitrile/dioxane, 2:1 (v/v)). Found: C, 59.2; H, 8.4; N, 9.9%. Calcd. for C₂₈H₄₈N₄O₆S (568.8): C, 59.1; H, 8.5; N, 9.85%. δ_{H} (400 MHz; DMSO-*d*₆) 8.54 (2H, t, *J* = 5.6 Hz, 2 NH), 7.66 (2H, s, 2 CH), 6.78–6.68 (2H, m, 2 NH), 3.25–3.15 (4H, m, 2 CH₂), 2.93–2.83 (4H, m, 2 CH₂), 1.54–1.42 (4H, m, 2 CH₂), 1.39–1.32 (4H, m, 2 CH₂), 1.36 (18H, s, 2 C(CH₃)₃), 1.29–1.20 (8H, m, 4 CH₂). δ_{C} (101 MHz, DMSO-*d*₆) 160.6, 155.6, 143.2, 127.9, 77.4, 39.8, 39.2, 29.5, 29.1, 28.3, 26.2, 26.0. *m/z* (MS-ESI) 591.30 (M+Na)⁺.

Di-*tert*-butyl (((((thiophene-2,5-dicarbonyl)bis(azanediyl))bis(ethane-2,1-diyl))bis(oxy))bis(ethane-2,1-diyl))dicarbamate (1b) (76%) was obtained similarly to **1a**. Starting *tert*-butyl (2-(2-aminoethoxy)ethyl)carbamate hydrochloride (1.25 equiv.) was preliminarily treated with DIPEA (10% excess) in dry THF (1 mL) in a separate vessel under argon, heated until almost clear solution formed, and then added to a reaction mixture *via* syringe through a rubber septum. The product was purified by recrystallization from acetonitrile. White solid, m.p. 138–139 °C (from acetonitrile). Found: C, 52.95; H, 7.45; N, 10.2%. Calcd. for C₂₄H₄₀N₄O₈S (544.7): C, 52.9; H, 7.4; N, 10.3%. δ_{H} (400 MHz; DMSO-*d*₆) 8.62 (2H, t, *J* = 5.2 Hz, 2 NH), 7.71 (2H, s, 2 CH), 6.82–6.62 (2H, m, 2 NH), 3.54–3.45 (4H, m, 2 CH₂), 3.43–3.34 (8H, m, 4 CH₂), 3.12–3.01 (4H, m, 2 CH₂), 1.36 (18H, s, 2 C(CH₃)₃). δ_{C} (101 MHz, DMSO-*d*₆) 161.3, 156.1, 143.6, 128.6, 78.08, 69.5, 69.1, 40.2, 39.7, 28.7. *m/z* (MS-ESI) 545.40 (MH)⁺.

The cleavage of the Boc-protecting group was performed using our previously reported protocol.¹ To a cooled 25 wt. % solution of HCl in dioxane (5 mL) the corresponding Boc-protected derivative **1a** or **1b** (0.32 mmol) was added. The resulting mixture was stirred until the completion of the reaction (TLC monitoring – CHCl₃/MeOH, 1:2 (v/v) as an eluent). The precipitate formed was filtered off, washed with dioxane (3 × 2 mL), and dried in a desiccator under vacuum to yield product **2a** or **2b** quantitatively which was used in further transformations as is.

6,6'-((Thiophene-2,5-dicarbonyl)bis(azanediyl))bis(hexan-1-aminium) dichloride (2a) (95%). White solid, m.p. 230–232 °C (from dioxane). Found: C, 48.9; H, 7.7; N, 12.7%. Calcd. for C₁₈H₃₄Cl₂N₄O₂S (441.5): C, 49.0; H, 7.8; N, 12.7%. δ_{H} (400 MHz; DMSO-*d*₆) 8.65 (2H, t, *J* = 5.2 Hz, 2 NH), 7.80 (6H, br. s, 2 NH₃⁺), 7.72 (2H, s, 2 CH), 3.26–2.16 (4H, m, 2 CH₂), 2.79–2.69 (4H, m,

2 CH₂), 1.59–1.44 (8H, m, 4 CH₂), 1.37–1.24 (8H, m, 4 CH₂). δ_c (101 MHz, DMSO-*d*₆) 160.7, 143.2, 128.1, 39.0, 38.7, 28.9, 26.9, 25.9, 25.5. *m/z* (MS-ESI) 369.49 (M–H⁺, 2Cl[–])⁺.

2,2'-((((Thiophene-2,5-dicarbonyl)bis(azanediyl))bis(ethane-2,1-diyl))bis(oxy))bis(ethane-1-aminium) dichloride (2b) (97%). White solid, m.p. 190–192 °C (from dioxane). Found: C, 40.3; H, 6.2; N, 13.4%. Calcd. for C₁₄H₂₆Cl₂N₄O₄S (417.4): C, 40.3; H, 6.3; N, 13.4%. δ_H (400 MHz; DMSO-*d*₆) 8.90 (2H, t, *J* = 5.6 Hz, 2 NH), 8.06 (6H, br. s, 2 NH₃⁺), 7.92 (2H, s, 2 CH), 3.63 (4H, t, *J* = 5.2 Hz, 2 CH₂), 3.60–3.55 (4H, m, 2 CH₂), 3.47–3.40 (4H, m, 2 CH₂), 3.02–2.92 (4H, m, 2 CH₂). δ_c (101 MHz, DMSO-*d*₆) 161.0, 143.1, 128.7, 68.8, 66.2, 38.9, 38.6. *m/z* (MS-ESI) 345.39 (M–H⁺, 2Cl[–])⁺.

Dyes **BAO-1**, **BAO-2** and **BAO-3** were synthesized using our previously reported protocol.¹

10,10'-((((Thiophene-2,5-dicarbonyl)bis(azanediyl))bis(ethane-2,1-diyl))bis(azanediyl))-bis(6-oxohexane-6,1-diyl))bis(3,6-bis(dimethylamino)acridin-10-ium) dichloride (BAO-1). ¹H and ¹³C spectral data are consistent with previously reported.¹ HRMS *m/z* (ESI⁺) C₅₆H₇₂N₁₀O₄S²⁺ (980.54477) calculated [M–2Cl[–]]²⁺ 490.27239, found *m/z*: 490.27249.

10,10'-((((Thiophene-2,5-dicarbonyl)bis(azanediyl))bis(hexane-6,1-diyl))bis(azanediyl))bis(6-oxohexane-6,1-diyl))bis(3,6-bis(dimethylamino)acridin-10-ium) dichloride (BAO-2) (45%). Dark red solid, m.p. 194–196 °C (from dioxane). Found: C, 66.15; H, 7.5; N, 12.1%. Calcd. for C₆₄H₈₈Cl₂N₁₀O₄S (1164.4): C, 66.0; H, 7.2; N, 12.3%. δ_H (400 MHz; DMSO-*d*₆) 8.75 (2H, s, H(9) and H(9')), 8.62–8.49 (2H, m, 2 NH), 7.90 (4H, d, *J* = 8.0 Hz, H(1), H(1'), H(8) and H(8')), 7.78–7.69 (2H, m, 2 NH), 7.65 (2H, s, 2 CH), 7.25 (4H, d, *J* = 8.0 Hz, H(2), H(2'), H(7) and H(7')), 6.61 (4H, s, H(4), H(4'), H(5) and H(5')), 4.75–4.57 (4H, m, 2 N⁺CH₂), 3.26 (24H, s, 4 N(CH₃)₂), 3.23–3.14 (8H, m, 4 CH₂), 3.04–2.94 (4H, m, 2 CH₂), 2.15–2.03 (4H, m, 2 C(O)CH₂), 1.91–1.79 (4H, m, 2 CH₂), 1.71–1.41 (12H, m, 6 CH₂), 1.39–1.17 (8H, m, 4 CH₂). δ_c (101 MHz, DMSO-*d*₆) 171.7, 160.6, 155.4, 143.2, 142.8, 142.1, 133.0, 127.8, 116.5, 114.4, 92.5, 46.6, 40.3, 40.2, 38.3, 35.2, 29.1, 29.0, 26.05, 26.08, 25.9, 25.3, 24.9. *m/z* (MS-ESI) 546.77 [M–2Cl[–]]²⁺. HRMS *m/z* (ESI⁺) C₆₄H₈₈N₁₀O₄S²⁺ (1092.66997) calculated [M–2Cl[–]]²⁺ 546.33499, found *m/z*: 546.33527.

10,10'-((((Thiophene-2,5-dicarbonyl)bis(azanediyl))bis(ethane-2,1-diyl))bis(oxy))bis(ethane-2,1-diyl))bis(azanediyl))bis(6-oxohexane-6,1-diyl))bis(3,6-bis(dimethylamino)acridin-10-ium) dichloride (BAO-3) (37%). Dark red solid, m.p. 188–190 °C (from dioxane). Found: C, 63.2; H, 7.2; N, 12.3%. Calcd. for C₆₀H₈₀Cl₂N₁₀O₆S (1140.3): C, 63.2; H, 7.1; N, 12.3%. δ_H (400 MHz; DMSO-*d*₆) 8.90–8.78 (2H, m, 2 NH), 8.62 (2H, s, H(9) and H(9')), 8.01–7.91 (2H, m, 2 NH), 7.80 (4H, d, *J* = 9.2 Hz, H(1), H(1'), H(8) and H(8')), 7.73 (2H, s, 2 CH), 7.16 (4H, d, *J* = 9.2 Hz, H(2), H(2'), H(7) and

H(7')), 6.47 (4H, s, H(4), H(4'), H(5) and H(5')), 4.66–4.45 (4H, m, 2 N⁺CH₂), 3.53–3.45 (4H, m, 2 OCH₂), 3.42–3.31 (8H, m, 4 NCH₂), 3.22 (24H, s, 4 N(CH₃)₂), 2.13 (4H, t, *J* = 6.2 Hz, 2 C(O)CH₂), 1.85–1.69 (8H, m, 4 CH₂), 1.69–1.57 (4H, m, 2 CH₂), 1.56–1.43 (4H, m, 2 CH₂). δ_c (101 MHz, DMSO-*d*₆) 172.1, 160.9, 155.2, 143.1, 142.6, 141.9, 132.9, 128.2, 116.4, 114.2, 92.3, 68.9, 68.6, 46.5, 40.2, 38.5, 35.1, 25.9, 25.2, 24.9, 23.5. *m/z* (MS-ESI) 534.91 [M–2Cl[–]]²⁺. HRMS *m/z* (ESI⁺) C₆₀H₈₀N₁₀O₆S²⁺ (1068.59720) calculated [M–2Cl[–]]²⁺ 534.29860, found *m/z*: 534.29889.

S2. Spectral measurements

S2.1. Absorption, fluorescence excitation and emission spectra

Absorption spectra were recorded for the dye concentrations (c_{Dye}) $\sim 1 \mu\text{M}$ in methanol, 10 mM Tris buffer (pH 8.0) or in presence of dsDNA ($c_{\text{DNA}} \sim 100 \mu\text{g/mL}$). All the absorption spectra were recorded in 1 cm quartz cells at 25 °C using a PerkinElmer Lambda 35 UV/Vis spectrophotometer. Absorption maxima were determined with an accuracy of $\pm 0.5 \text{ nm}$ and rounded off.

Molar absorptivity (ϵ). The dye (5–10 mg) was dissolved in the selected solvent (100 mL), the stock solution was diluted to the dye concentration $\sim 1 \mu\text{M}$ and the absorbance (A) at the absorption band maximum was measured in a 1 cm standard quartz cell. The molar absorptivities were calculated according to the Beer-Lambert law. The molar absorptivity of each dye was independently measured three times and the average value was taken. The reproducibility for determining the molar absorptivity was within $\pm 1,000 \text{ M}^{-1}\text{cm}^{-1}$.

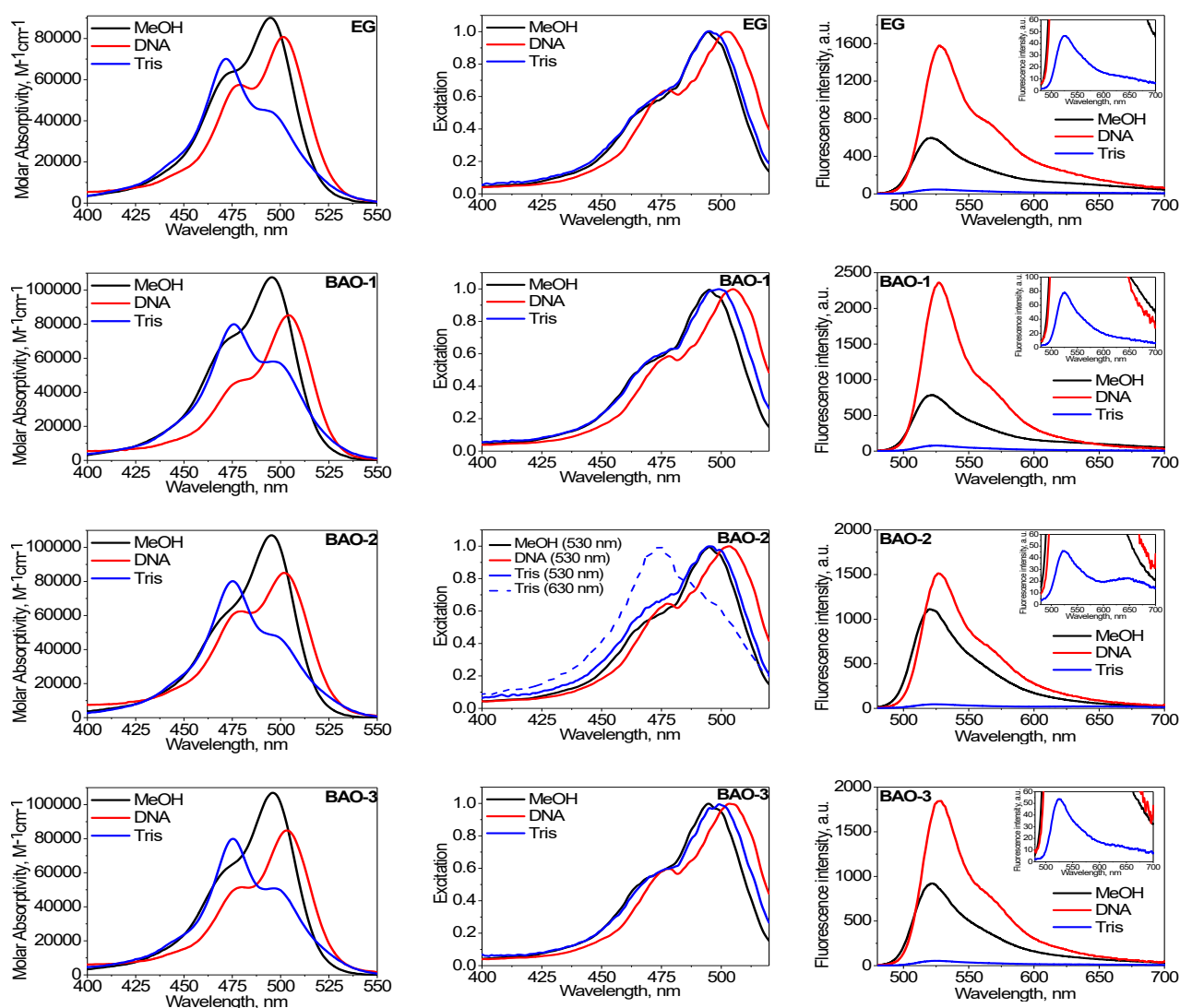
Emission spectra were measured for the dye concentration $\sim 1 \mu\text{M}$ in the selected solvent. The excitation wavelength was 470 nm. The fluorescence measurements were done in 1 cm standard quartz cells at 25 °C using a Varian Cary Eclipse spectrofluorometer. The emission spectra were corrected for wavelength-dependent instrument sensitivity. Emission maxima were determined with an accuracy of $\pm 1.0 \text{ nm}$.

Fluorescence quantum yields (Φ_{F}). The integrated relative intensities of the dyes were measured in 1 cm cells against acridine orange as the reference. The quantum yields were calculated according to [Equation S1](#).

$$\Phi_{\text{F}} = \Phi_{\text{F,AO}} \times (F / F_{\text{AO}}) \times (A_{\text{AO}} / A) \times (n_{\text{D(media),AO}}^2 / n_{\text{D(media)}}^2), \quad (\text{S1})$$

where $\Phi_{\text{F,AO}}$ is the quantum yield of **AO** ($\Phi_{\text{F,AO}} = 25\%$ in 5 mM phosphate buffer, pH 6.9),⁴ F_{AO} and F are the areas (integral intensities) of the emission spectra ($F = \int I(\lambda)d(\lambda)$) of **AO** and the dye under examination, respectively; A_{AO} and A are the absorbencies at the excitation wavelength of **AO** and the dye under examination, respectively; $n_{\text{D(media),AO}}$ and $n_{\text{D(media)}}$ are the refractive indices of the solvent, where the reference **AO** and the dye under examination are dissolved, respectively.

The quantum yield of each sample was independently measured 3–4 times and the average value was taken. The reproducibility was within 5%.



Supplementary Figure S1. Absorption (left), fluorescence excitation (middle) and emission (right) spectra of commercial **EG** and obtained **BAO-1**, **BAO-2** and **BAO-3** dyes ($C_{\text{Dye}} = 1 \mu\text{M}$) free in 10 mM Tris-buffer pH 8.0 (blue line), in MeOH (black line) and in the presence of DNA ($C_{\text{DNA}} = 100 \mu\text{g/mL}$) (red line). Inserts on the emission spectra show the scaled-up emission spectra of the dyes in Tris-buffer pH 8.0.

S2.2. Fluorescence lifetimes

Fluorescence lifetimes (τ) were acquired with ChronosDFD (ISS, Champaign, IL), a frequency domain lifetime spectrofluorometer, using a 488-nm laser diode as an excitation light source and a 520-nm long-pass emission filter. The measurements were done against fluorescein in 0.1 M NaOH as a reference ($\tau = 4.10 \text{ ns}$) at 25 °C.^{5,6} DFD acquisition model K520 provided modulation frequencies in the range from 9 KHz to 1.2 GHz; the laser diode was driven directly at a frequency f' . The gain of the light detector was driven at a frequency ($f' + \Delta f'$), where the quantity $\Delta f'$, called the cross-correlation frequency, was of the order of 1 KHz. The signals of the sum (that is $2f' + \Delta f'$)

and the difference (that is $\Delta f'$) of the two frequencies were recorded and the low frequency component $\Delta f'$ was taken to determine DC (direct current), AC (alternating current) and the phase components of the signal. In all lifetime measurements the dye concentrations were $\sim 1 \mu\text{M}$. Instrument control, data acquisition and data analysis were performed using Vinci Beta 3.1 – Multidimensional Fluorescence Spectroscopy software (ISS, Champaign, IL). The analysis of the time-resolved fluorescence data was carried out using the traditional non-linear least squares method. This method evaluates how close a model selected by the user matches the data acquired with the instrument. The Marquardt–Levenberg algorithm was utilized for the minimization routine of the χ^2 -function that compares the selected model with the experimental data. Frequency-domain data were used to determine the lifetimes using the multi-exponential model expressed by [Equation S2](#).⁷

$$I(t) = \sum_{i=1}^n \alpha_i e^{-t/\tau_i}, \quad (\text{S2})$$

where α_i is the pre-exponential factor, τ_i the lifetime, and $n = 1$ or 2 for the single or double exponential fits, respectively. The fractional contribution of each component in the intensity decay $I(t)$ is given by [Equation S3](#).⁷

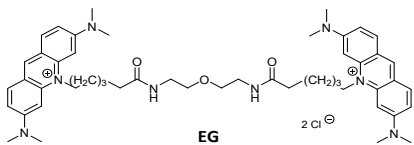
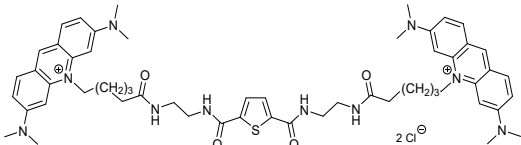
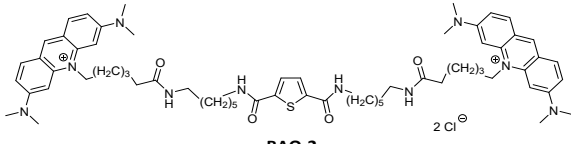
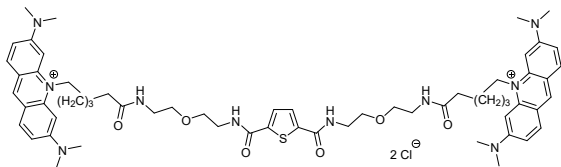
$$f_i = \alpha_i \tau_i / \sum_j \alpha_j \tau_j, \quad (\text{S3})$$

The mean lifetime (τ_{mean}) for a two-exponential decay was determined according to the [Equation S4](#).⁷

$$\tau_{mean} = f_1 \tau_1 + f_2 \tau_2, \quad (\text{S4})$$

where f_1 and f_2 are the fractional intensities, τ_1 and τ_2 are the lifetimes.

Supplementary Table S1. Fluorescence decay parameters: f_1 and f_2 are the fractional intensities, τ_1 and τ_2 are the lifetimes corresponding to each of the component of the two-exponential model, χ^2 is a statistical parameter, τ_{mean} is the mean lifetime of dimeric dyes at $c_{Dye} = 1 \mu\text{M}$, and dye–dsDNA complexes with $100 \mu\text{g/mL}$ dsDNA at $T = 25 \text{ }^\circ\text{C}$.

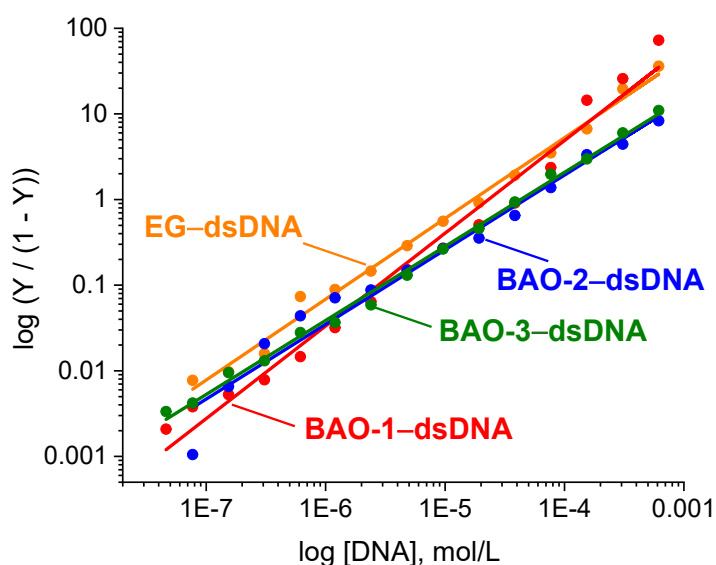
Dye	Media	τ_1 , ns	f_1	τ_2 , ns	f_2	χ^2	τ_{mean} , ns
 <p>EG</p>	Tris buffer	1.99	0.63	0.41	0.37	1.54	1.40
	MeOH	2.54	0.50	0.74	0.50	2.10	1.65
	dsDNA	6.46	0.74	2.49	0.26	1.28	5.41
 <p>BAO-1</p>	Tris buffer	2.11	0.55	0.39	0.45	1.47	1.33
	MeOH	2.19	0.60	0.60	0.40	1.17	1.56
	dsDNA	5.45	0.76	2.27	0.25	0.96	4.67
 <p>BAO-2</p>	Tris buffer	2.23	0.55	0.17	0.45	1.55	1.30
	MeOH	2.09	0.69	0.55	0.31	0.98	1.61
	dsDNA	5.51	0.76	1.55	0.24	1.08	4.54
 <p>BAO-3</p>	Tris buffer	2.33	0.53	0.08	0.47	2.31	1.26
	MeOH	2.22	0.62	0.63	0.39	1.22	1.61
	dsDNA	5.84	0.68	2.44	0.32	1.33	4.76

S2.3. Binding constants

Binding constants (K_b) for the studied dyes and dsDNA were determined by using fluorescence titration method.⁸ A series of 15 solutions with different dsDNA concentrations were prepared by diluting the initial dsDNA solution, which had a concentration of 800 $\mu\text{g}/\text{mL}$, each time in twofold. All solutions of dsDNA were prepared in 10 mM Tris buffer (pH 8.0). Aliquots of the stock dye solution in DMSO were added to both the dsDNA solutions and the 10 mM Tris buffer. The volume of the aliquot was selected to provide the dye concentration in the final solution to be $\sim 1.5 \mu\text{M}$. The integrated relative intensity of the dye fluorescence signal was registered for each dsDNA-dye solution at the excitation wavelength of 450 nm. To build the appropriate binding isotherm, the measured fluorescence intensities were plotted against the concentration of dsDNA. To obtain the values of dye-dsDNA binding constants, Hill equation was used as an instrument to describe the degree of cooperativity in ligand (dye) binding to a macromolecule with multiple binding sites (dsDNA).⁹ In particular, the rearrangement of the Hill equation into a straight line (Figure S2 (ESI⁺), Equation S5) was used:

$$\log (Y / (1 - Y)) = n \times \log [\text{DNA}] + \log K_b, \quad (\text{S5})$$

where Y is the fractional saturation calculated as $((F - F_0) / (F_{max} - F))$ (F is the fluorescence intensity at a given concentration of dsDNA, F_0 is the initial fluorescence intensity of the dye without dsDNA, and F_{max} is the maximum fluorescence intensity in presence of dsDNA); $[\text{DNA}]$ is the molar concentration of dsDNA in terms of base pairs (bp); n is the Hill coefficient, which indicates cooperativity; K_b is the binding constant. The calculation of dsDNA concentration in terms of bp from a concentration given in $\mu\text{g}/\text{mL}$ is based on the assumption that the average weight of a bp is 650 g/mol.¹⁰ Parameters n and K_b were determined from the slope and the ordinate intercept of Equation S5 respectively. The binding constants for each dye were independently determined 3 times and the average values were taken.



Supplementary Figure S2. Rearrangement of the Hill equation into a straight line for **EG** and **BAO** dyes: Y is the fractional saturation calculated as $((F - F_0) / (F_{\max} - F_0))$ (F is the fluorescence intensity at a given concentration of dsDNA, F_0 is the initial fluorescence intensity of the dye without dsDNA, and F_{\max} is the maximum fluorescence intensity in presence of dsDNA; $[DNA]$ is the molar concentration (mol/L) of dsDNA in terms of base pairs).

S2.4. Brightness and stability tests

The brightness (B) in methanol, 10 mM Tris buffer (pH 8.0) and in the presence of dsDNA ($C_{DNA} \sim 100 \mu\text{g/mL}$) was calculated according to Equation S6.

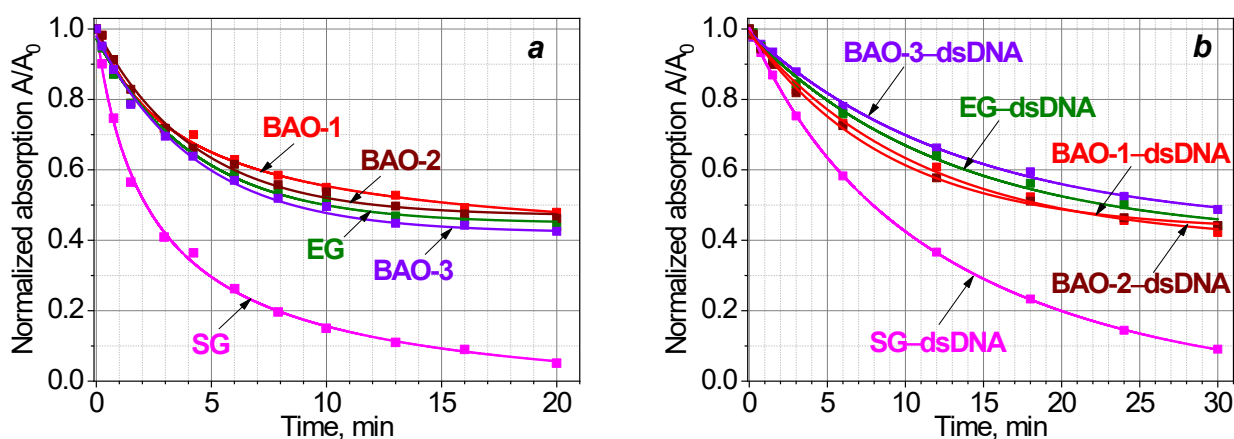
$$B = \varepsilon \times \Phi_F / 100, \quad (\text{S6})$$

where ε is the molar absorptivity at a specific wavelength (488 nm for **EG** and dimeric **BAO** dyes), in $\text{M}^{-1}\text{cm}^{-1}$ and Φ_F is the fluorescence quantum yield, in %.

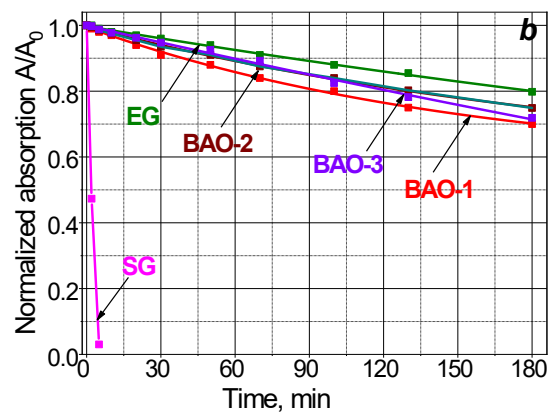
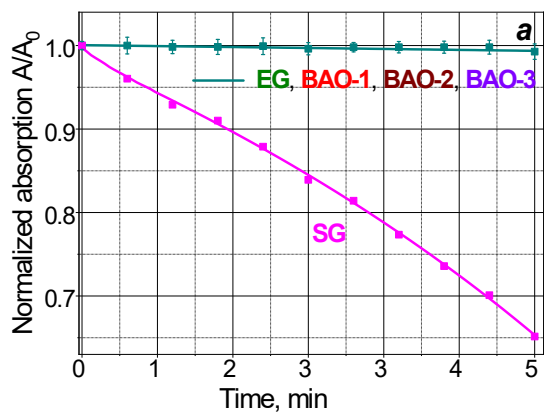
Photostability was measured for the dye concentrations of 1 μM in 10 mM Tris buffer (pH 8.0). Solutions with absorbance in the range between 0.095 and 0.10 (measured in standard 1 cm quartz cells) at the excitation wavelength were prepared. The samples were placed at the distance of 30 cm and exposed to light of metal-halogen lamp Philips HPI-T Plus 400W/645 at 60 °C. The samples were cooled to room temperature before the measurements. The absorption spectra of the solutions were measured before irradiation and during light exposure in different time frames. The photostability experiment for each sample was done 3 times and the average decay curve was obtained. Relative photostabilities were calculated as the ratio between the measured absorbances at the long-wavelength maximum before and after the light exposure (A/A_0).

Thermal stability was investigated by incubating the dye solutions ($c_{\text{Dye}} = 1 \mu\text{M}$) in 10 mM Tris buffer (pH 8.0) at 90 °C for 5 hours. Before the incubation at 90 °C and every 30 minutes during the incubation, the aliquots (20 μL) of the dye solution were taken, diluted in 2.98 mL of 10 mM Tris buffer (pH 8.0) to obtain a dye concentration of 1 μM , and the absorption spectra were measured at room temperature in a standard 1 cm quartz cuvette. Thermal stability was calculated as the ratio between the measured absorbances at the long-wavelength maximum before and after incubation (A/A_0).

Chemical stability was determined by keeping the dye solutions ($c_{\text{Dye}} = 1 \mu\text{M}$) in the solution of 8% H_2O_2 in 10 mM Tris buffer (pH 8.0) for 3 h at room temperature. Solution of 8% H_2O_2 in 10 mM Tris buffer (pH 8.0) was prepared by diluting the solution of 30% H_2O_2 with 13.6 mM Tris buffer (pH 8.0). The absorption spectra were measured at 24 °C on a PerkinElmer Lambda 35 UV/Vis spectrophotometer in a standard 1 cm quartz cuvette at certain intervals. Chemical resistance against the oxidizing reagent was calculated as the ratio between the measured absorbances at the long-wavelength maximum of each dye in 10 mM Tris buffer (pH 8.0) and in the solution of 8% H_2O_2 in 10 mM Tris buffer (pH 8.0) (A/A_0).



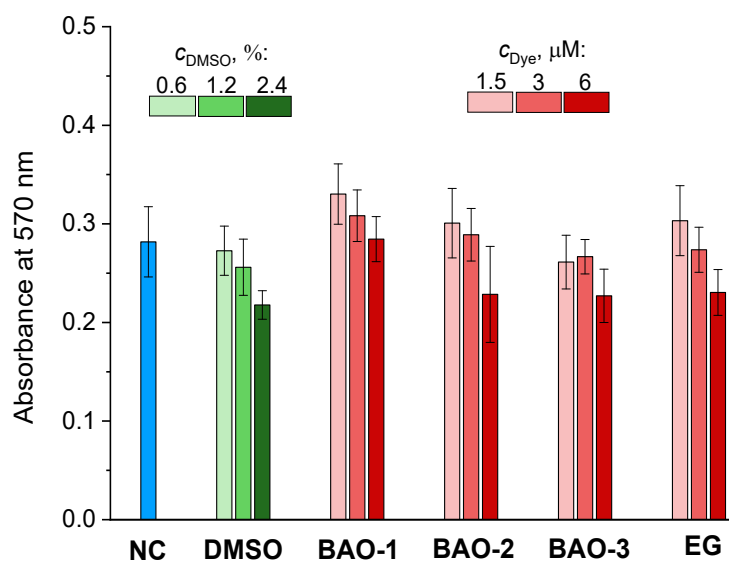
Supplementary Figure S3. Changes in the relative absorption (A/A_0) of EG, SYBR Green I (SG) and BAO dyes (a), and dye-dsDNA complexes (b) in 10 mM Tris buffer (pH 8.0) upon irradiation with a metal-halogen lamp, ($c_{\text{Dye}} = 1 \mu\text{M}$, $c_{\text{DNA}} = 100 \mu\text{g/mL}$).



Supplementary Figure S4. Changes in the relative absorption (A/A_0) of EG, SYBR Green I (SG) and BAO dyes ($c_{Dye} = 1 \mu M$) in 10 mM Tris buffer (pH 8.0) during the incubation at 90 °C (**a**) and in the solution of 8 % H_2O_2 during the incubation for 3 hours at 24 °C (**b**), ($c_{Dye} = 1 \mu M$).

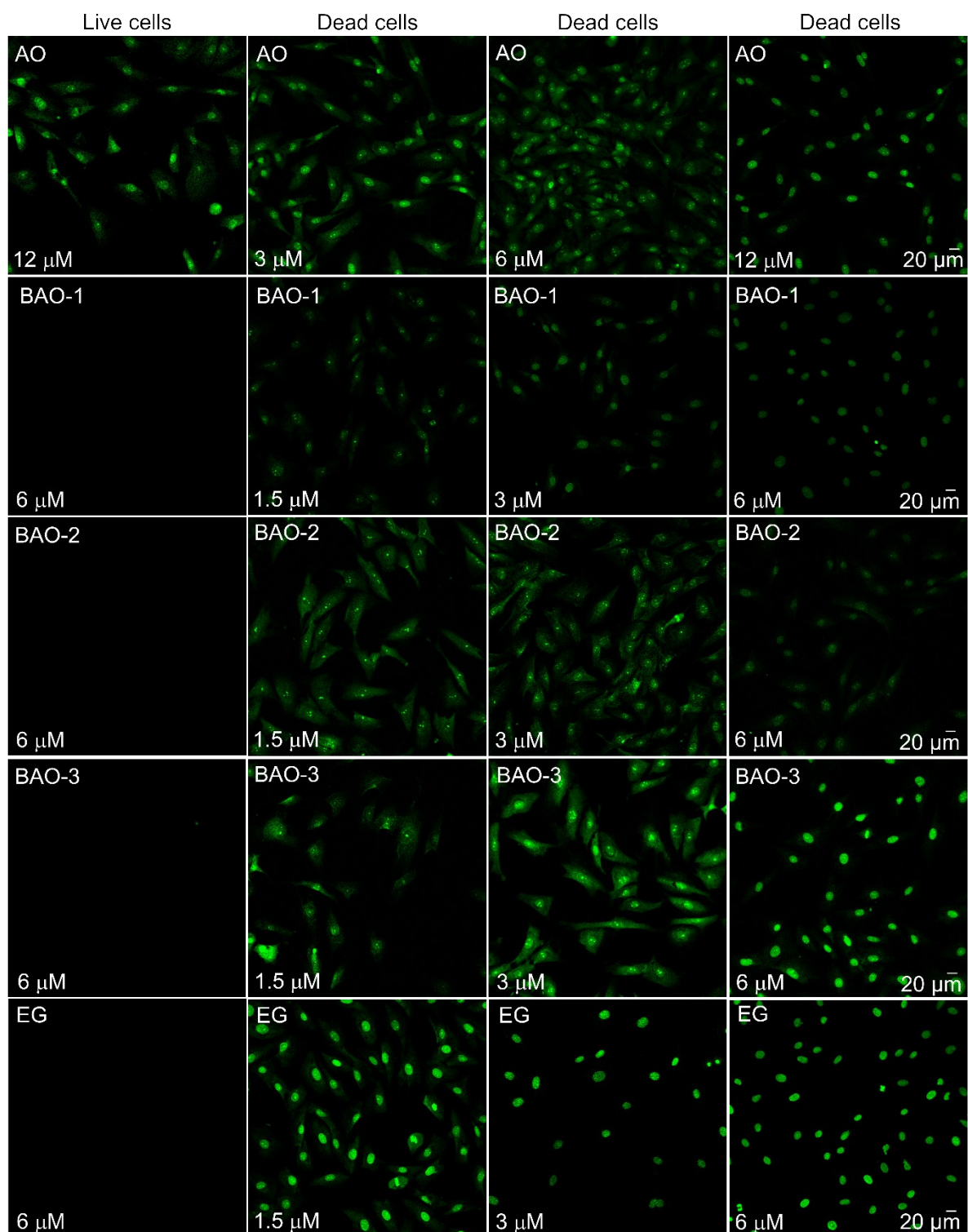
S3. Cell imaging

S3.1. Cytotoxicity assay

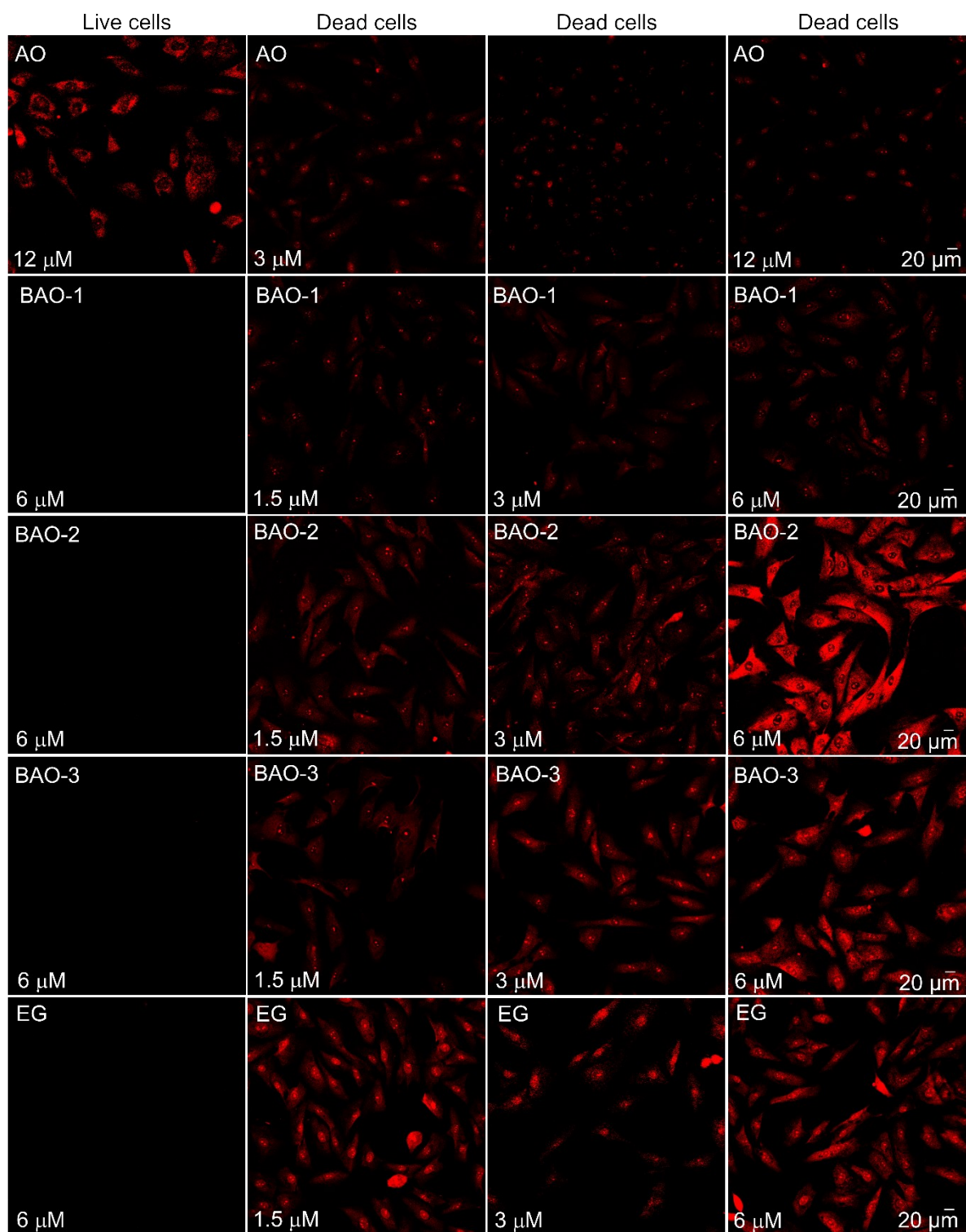


Supplementary Figure S5. Cytotoxic effect of dimeric dyes at dye concentrations 1.5 μM, 3 μM, 6 μM with 0.6 %, 1.2 %, 2.4 % DMSO, respectively on cultured rat fibroblasts assessed by MTT test.^{11,12} Untreated fibroblasts were used as a negative control (NC). Green columns show the cytotoxic effect of corresponding concentration of DMSO in staining solution.

S3.2. Results of confocal laser scanning microscopy

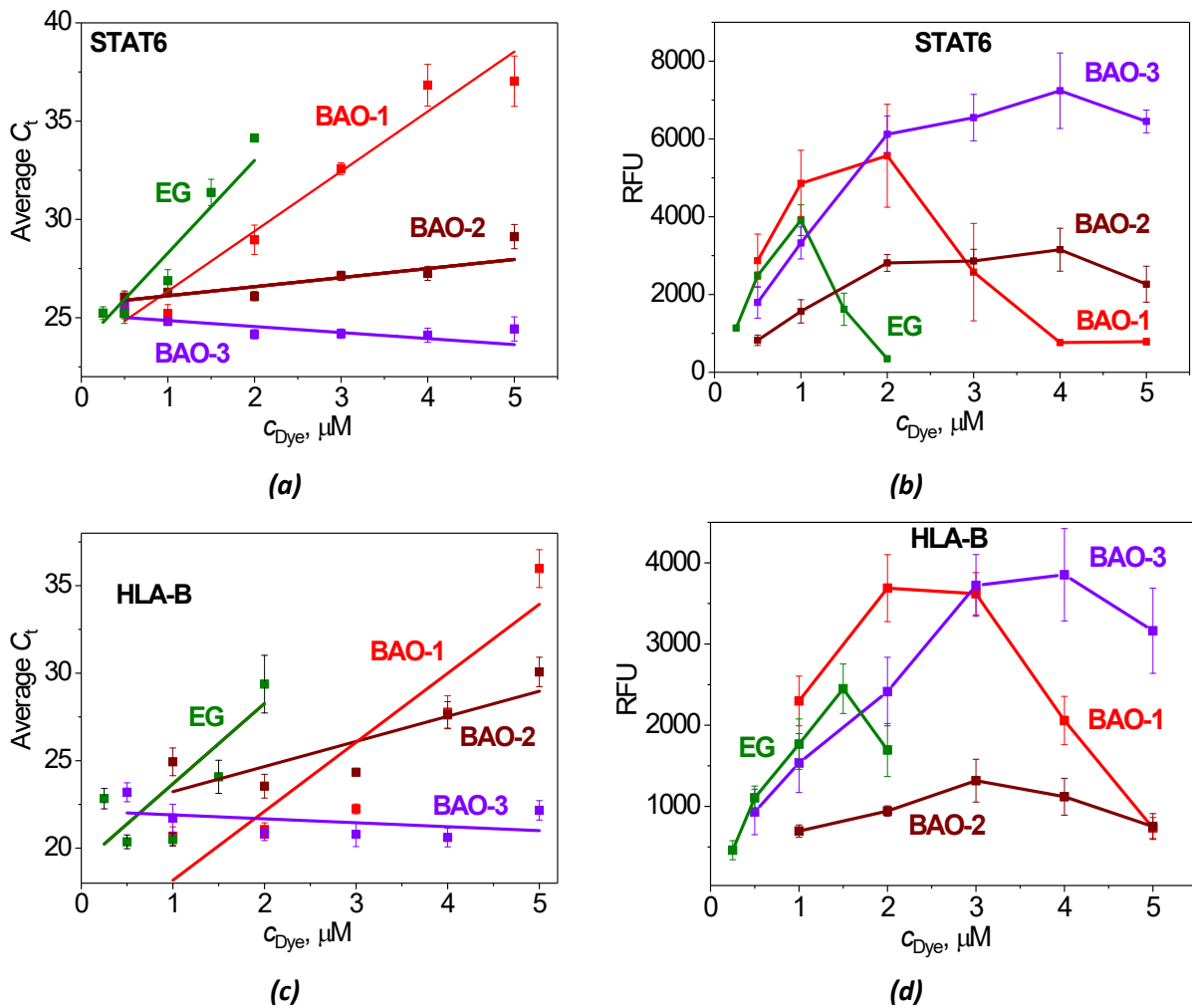


Supplementary Figure S6. Laser scanning confocal microscopy images of live and dead fibroblast cells incubated for 30 minutes with different concentrations of **AO**, **EG** and **BAO** dyes without washing. The laser excitation wavelength was 488 nm, and the fluorescence was recorded in green channel (detection ranges were set between 508–550 nm).

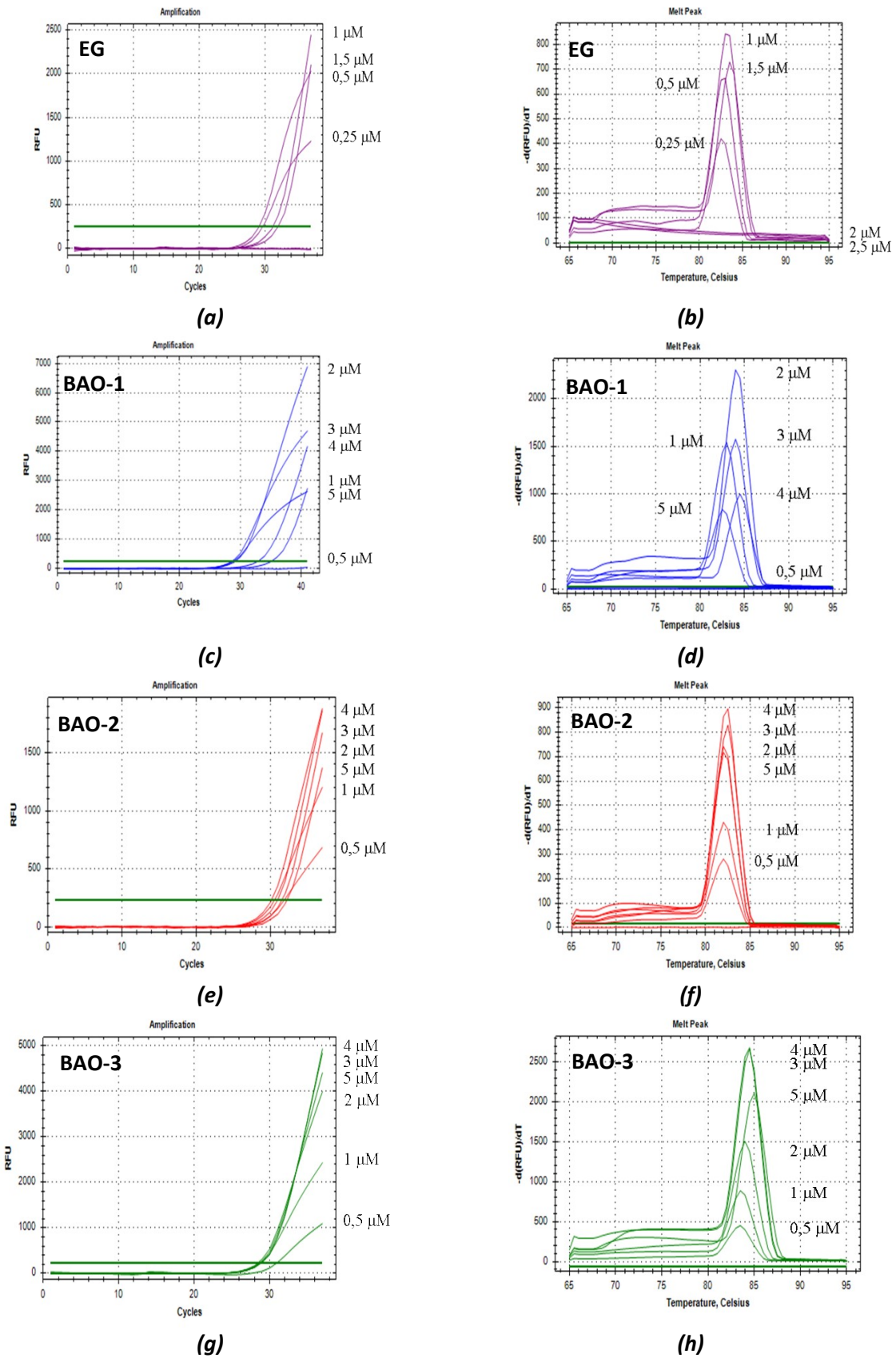


Supplementary Figure S7. Laser scanning confocal microscopy images of live and dead fibroblast cells incubated for 30 minutes with different concentrations of **AO**, **EG** and **BAO** dyes without washing. The excitation wavelength of the laser was 488 nm, and the fluorescence was recorded in red channel (detection ranges were set between 583–700 nm).

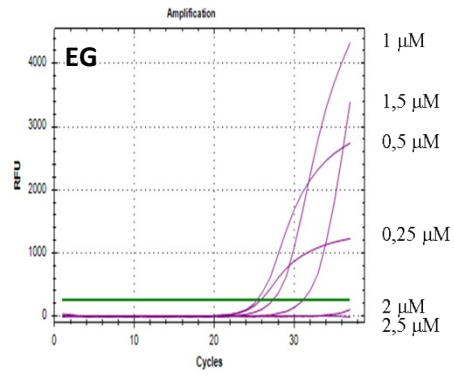
S4. qPCR experiments



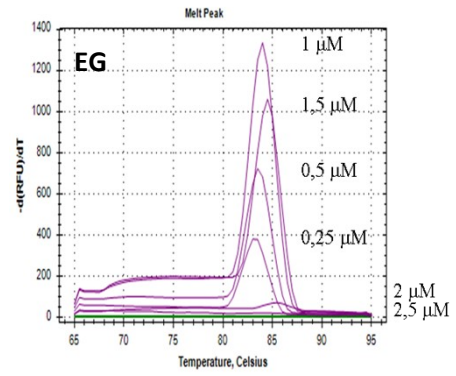
Supplementary Figure S8. Effect of dye concentration on (a, c) the average cycle threshold (C_t) value and (b, d) the end-point fluorescence intensity in relative fluorescence units (RFU) on dye concentration upon the amplification of STAT6 (a, b) and HLA-B (c, d) genes. Only points without significant PCR inhibition were included in the linear fits. The slope of the trendline from the fit is as follows for STAT6: EG: 4.71 ± 0.43 , BAO-1: 3.05 ± 0.25 , BAO-2: 0.46 ± 0.14 , BAO-3: -0.31 ± 0.13 ; and as follows for HLA-B: EG: 4.59 ± 1.60 , BAO-1: 3.94 ± 0.90 , BAO-2: 1.43 ± 0.53 , BAO-3: -0.23 ± 0.27 .



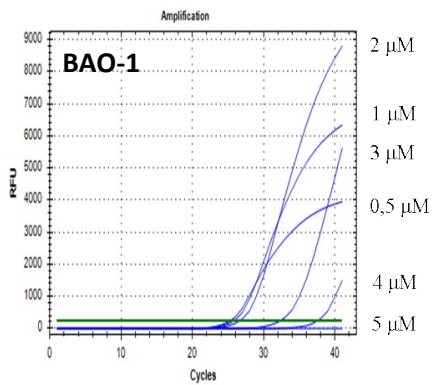
Supplementary Figure S9. Amplification curves (*a, c, e, g*) and the product melting curves (*b, d, f, h*) in the presence of EG ($c_{\text{Dye}} = 0.25, 0.5, 1.0, 1.5 \mu\text{M}$), and BAO-1, BAO-2, BAO-3 ($c_{\text{Dye}} = 0.5, 1.0, 2.0, 3.0, 4.0, 5.0 \mu\text{M}$) upon the amplification of STAT4 gene.



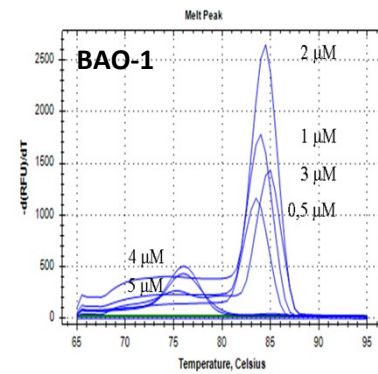
(a)



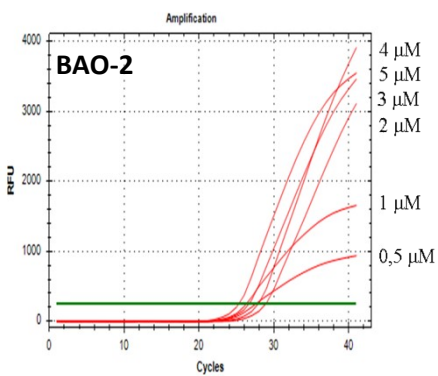
(b)



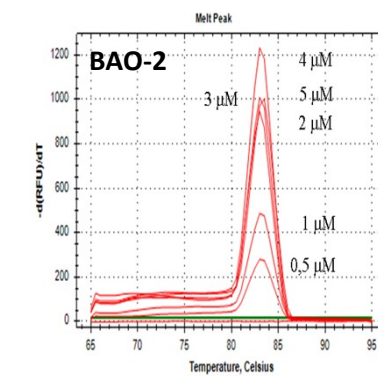
(c)



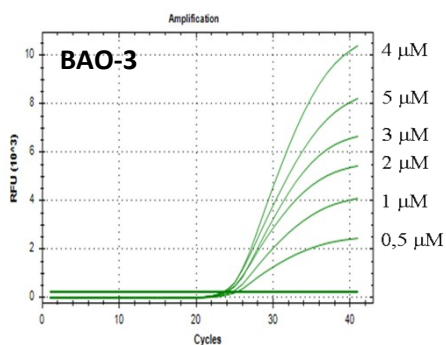
(d)



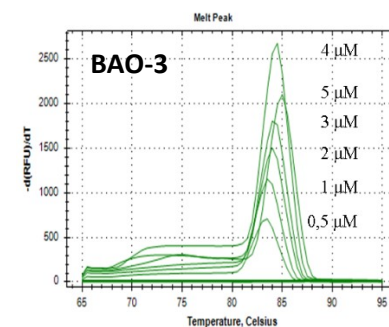
(e)



(f)

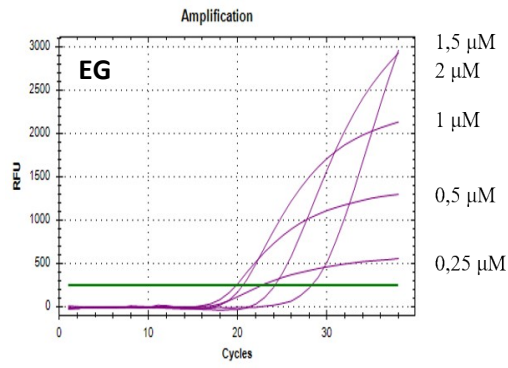


(g)

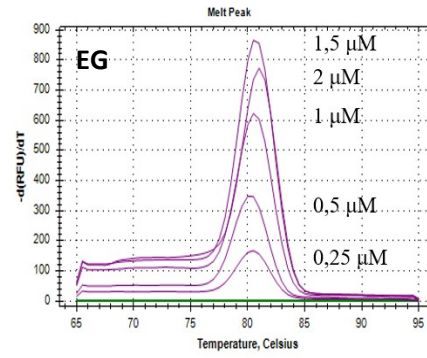


(h)

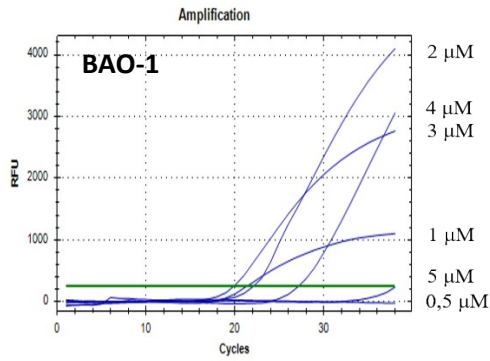
Supplementary Figure S10. Amplification curves (a, c, e, g) and the product melting curves (b, d, f, h) in the presence of EG, BAO-1, BAO-2 and BAO-3 upon the amplification of STAT6 gene.



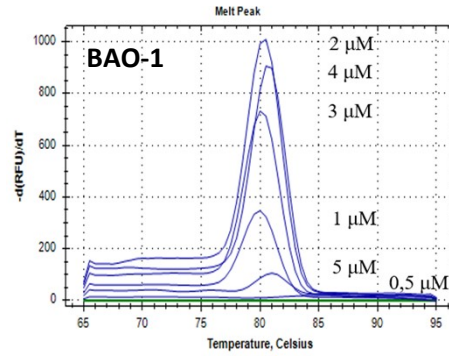
(a)



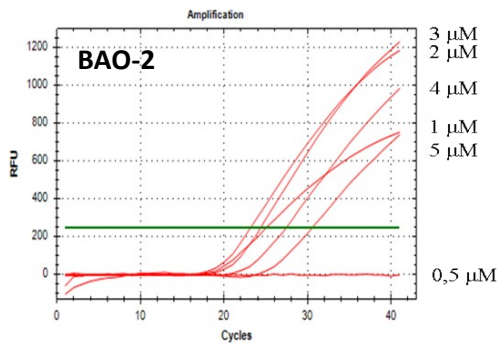
(b)



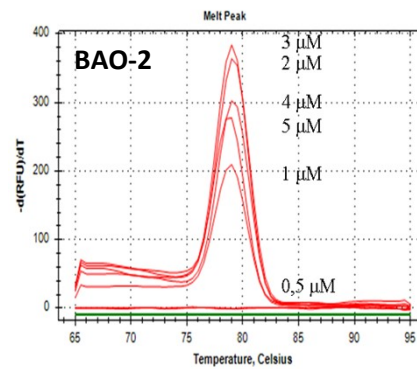
(c)



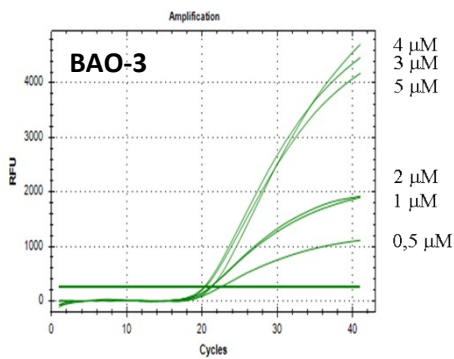
(d)



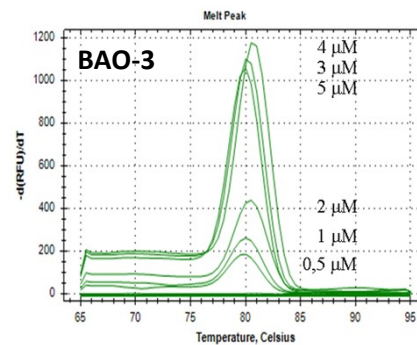
(e)



(f)



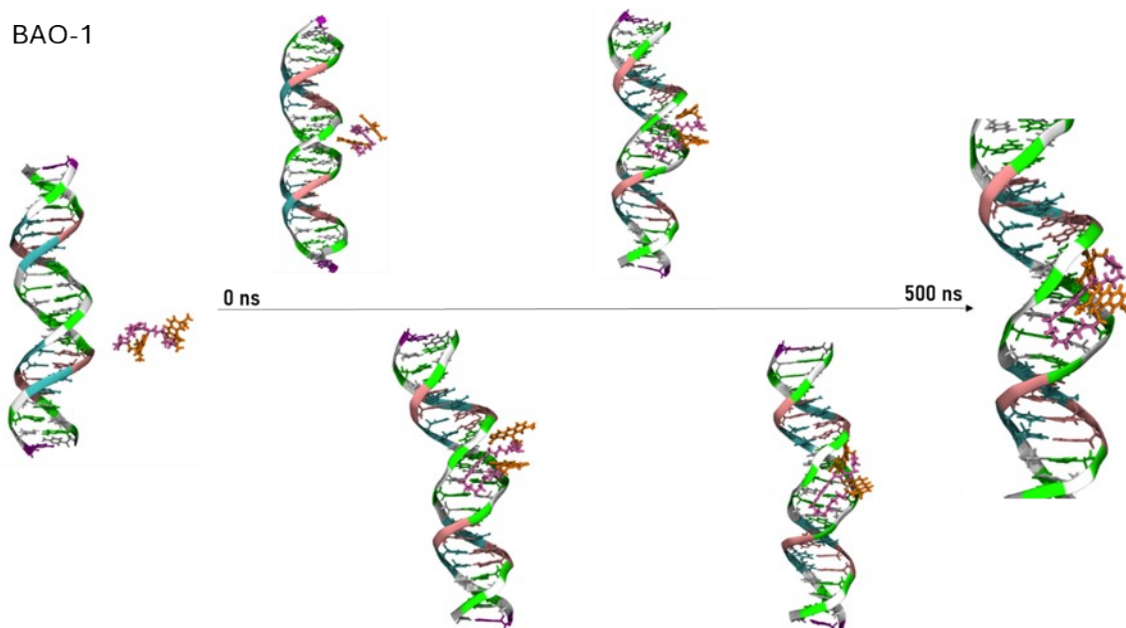
(g)



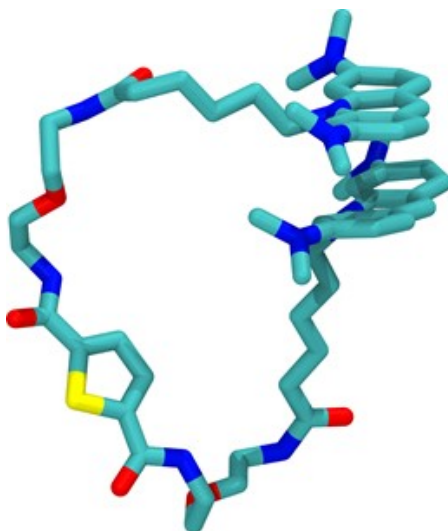
(h)

Supplementary Figure S11. Amplification curves (a, c, e, g) and the product melting curves (b, d, f, h) in the presence of EG, BAO-1, BAO-2 and BAO-3 upon the amplification of HLA-B gene.

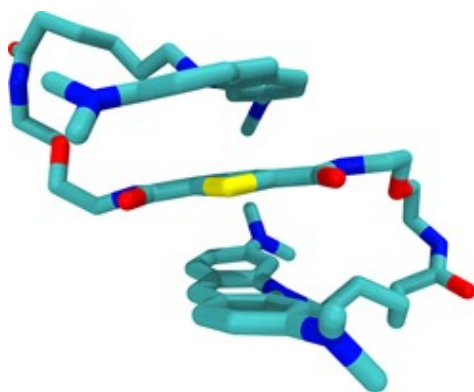
S5. MD simulations



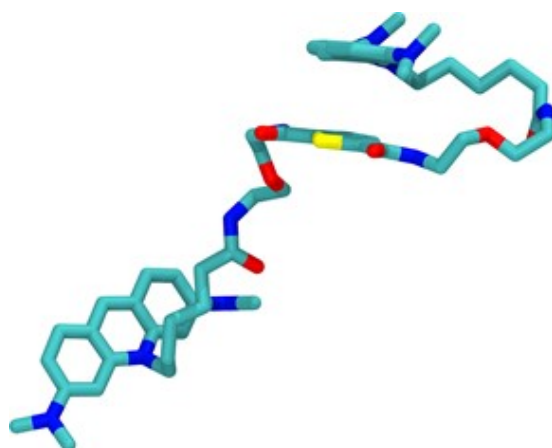
Supplementary Figure S12. Formation of the complex between **BAO-1** with dsDNA over 500 ns. Color code: guanine in green, cytosine in white, thymine in cyan and adenine in pink. The AO moieties of the dye are orange and the linker between them is purple.



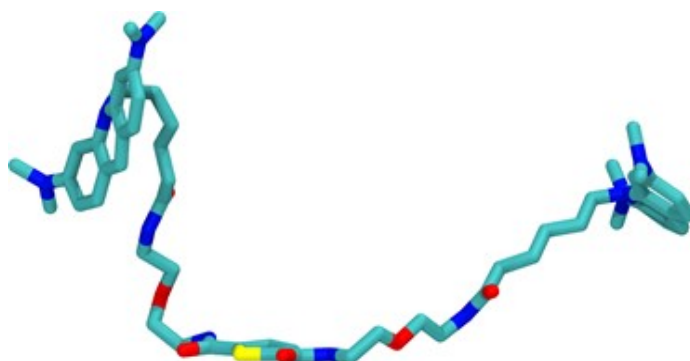
Supplementary Figure S13. Enlarged view of Inlet I1 from Figure 9 (in the article), depicting the **BAO-3** dye with the two stacked AO moieties. Color code: cyan are carbon atoms, blue are nitrogen atoms, red are oxygen atoms, and yellow is the sulphur atom. Hydrogen atoms are omitted for clarity.



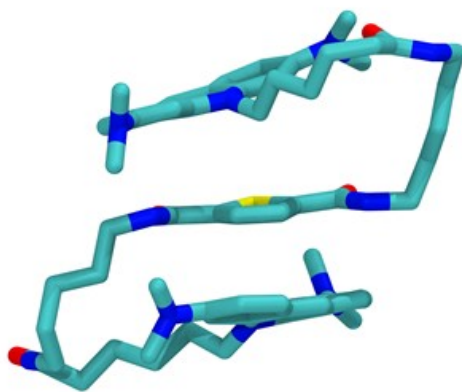
Supplementary Figure S14. Enlarged view of Inlet I2 from Figure 9 (in the article), depicting the **BAO-3** dye in the 3-components stacked conformation, stacking that is present in **BAO** dyes at a distance of 6-8 Å between the AO moieties. The color code is the same as in Supplementary Figure S13.



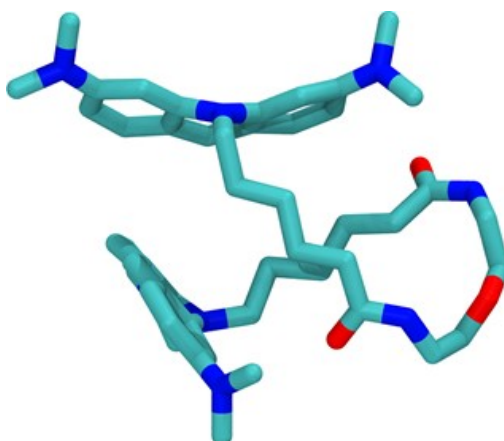
Supplementary Figure S15. Enlarged view of Inlet I3 from Figure 9 (in the article), depicting the conformation of the **BAO-3** dye at a distance between the two AO moieties of 1.5 Å. The color code is the same as in Supplementary Figure S13.



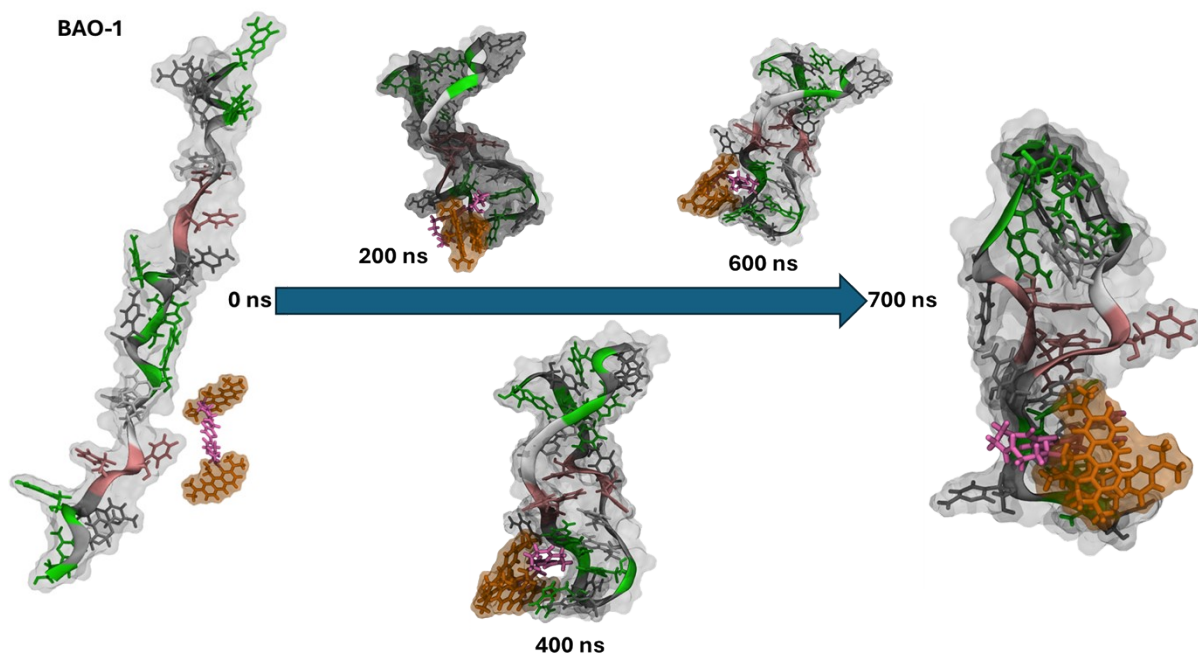
Supplementary Figure S16. Enlarged view of Inlet I4 from Figure 9 (in the article), depicting the conformation of the fully extended **BAO-3** dye at a distance between the two AO moieties of 24 Å. The color code is the same as in Supplementary Figure S13.



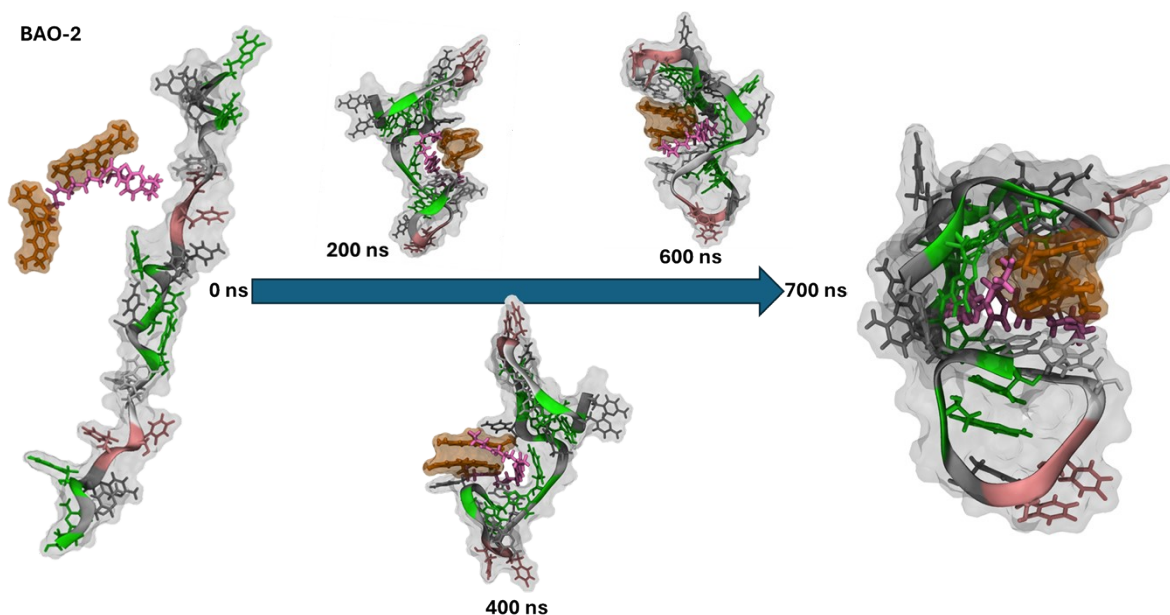
Supplementary Figure S17. Enlarged view of Inlet 15 from Figure 9 (in the article), depicting the conformation of the 3-components stacked **BAO-2** dye at a distance between the two AO moieties of 6-8 Å. The color code is the same as in Supplementary Figure S13.



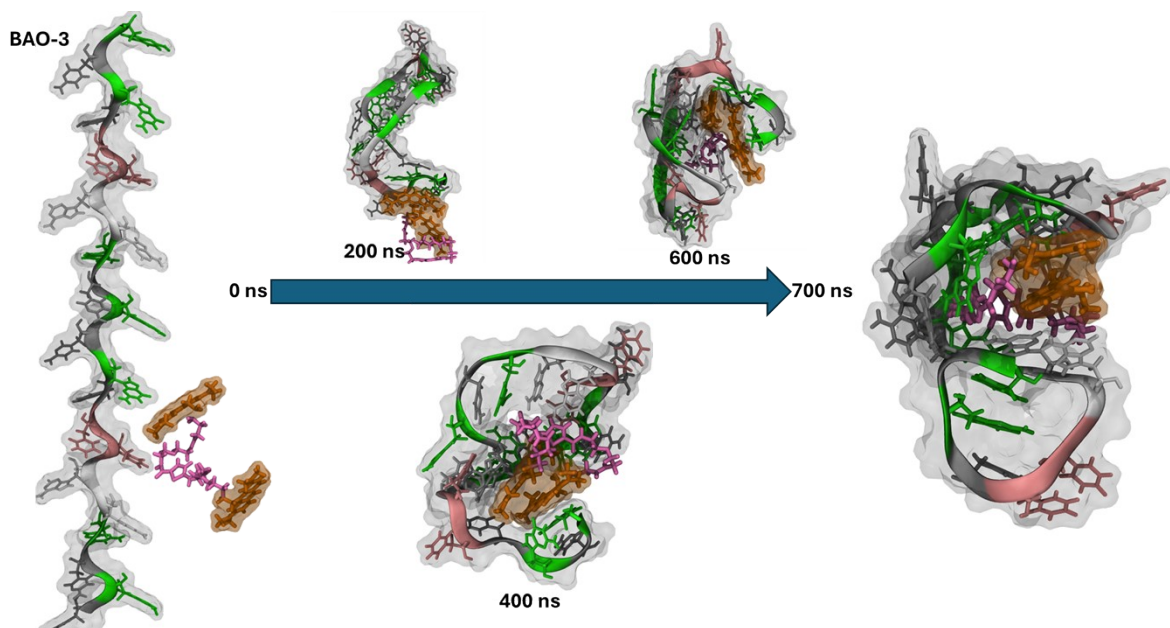
Supplementary Figure S18. Enlarged view of Inlet 16 from Figure 9 (in the article), depicting the conformation of the **EG** dye at a distance between the two AO moieties of 6-8 Å. The color code is the same as in Supplementary Figure S13.



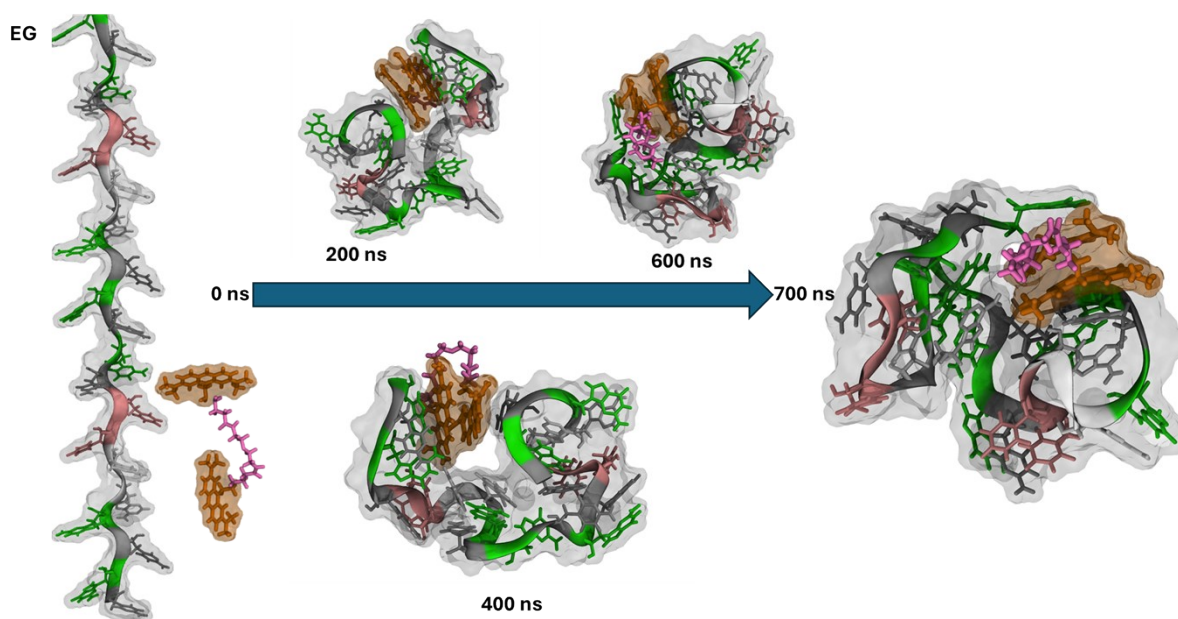
Supplementary Figure S19. Formation of the complex between **BAO-1** with RNA over 700 ns. Color code: guanine in green, adenine in white, cytosine in grey and uracil in pink. The AO moieties of the dye are orange and the linker between them is purple.



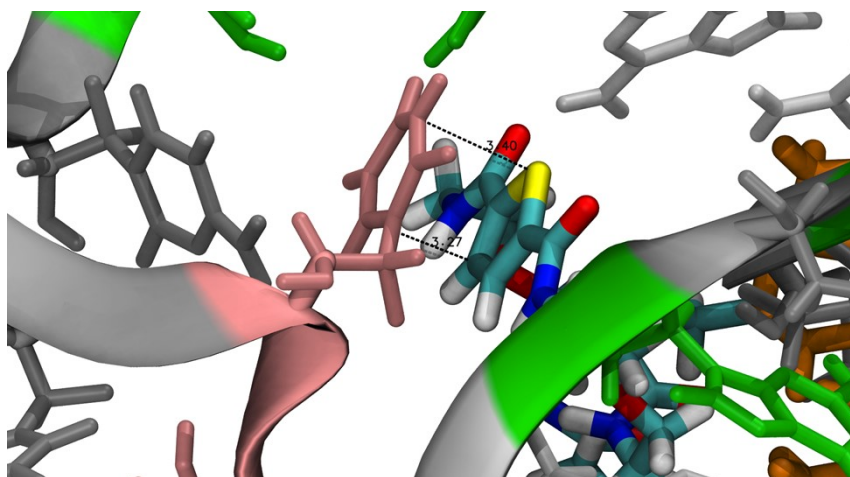
Supplementary Figure S20. Formation of the complex between **BAO-2** with RNA over 700 ns. Color code: guanine in green, adenine in white, cytosine in grey and uracil in pink. The AO moieties of the dye are orange and the linker between them is purple.



Supplementary Figure S21. Formation of the complex between **BAO-3** with RNA over 700 ns. Color code: guanine in green, adenine in white, cytosine in grey and uracil in pink. The AO moieties of the dye are orange and the linker between them is purple.

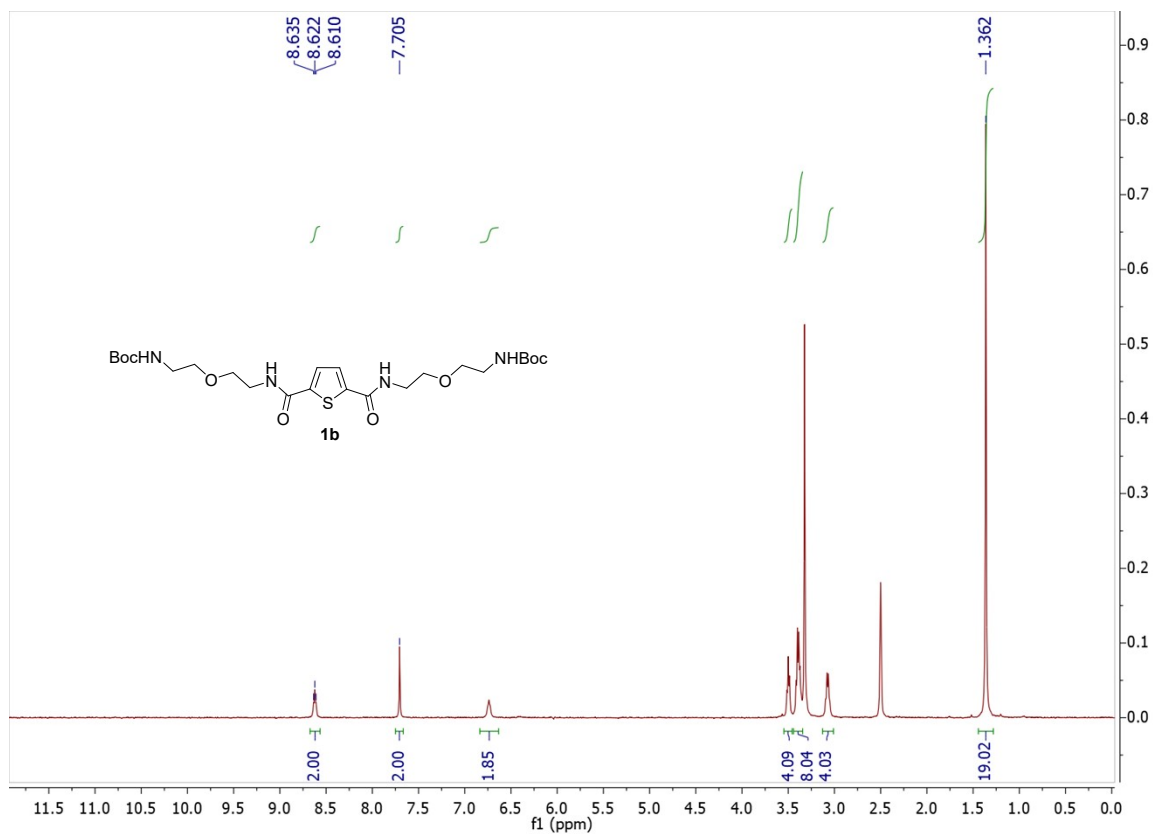
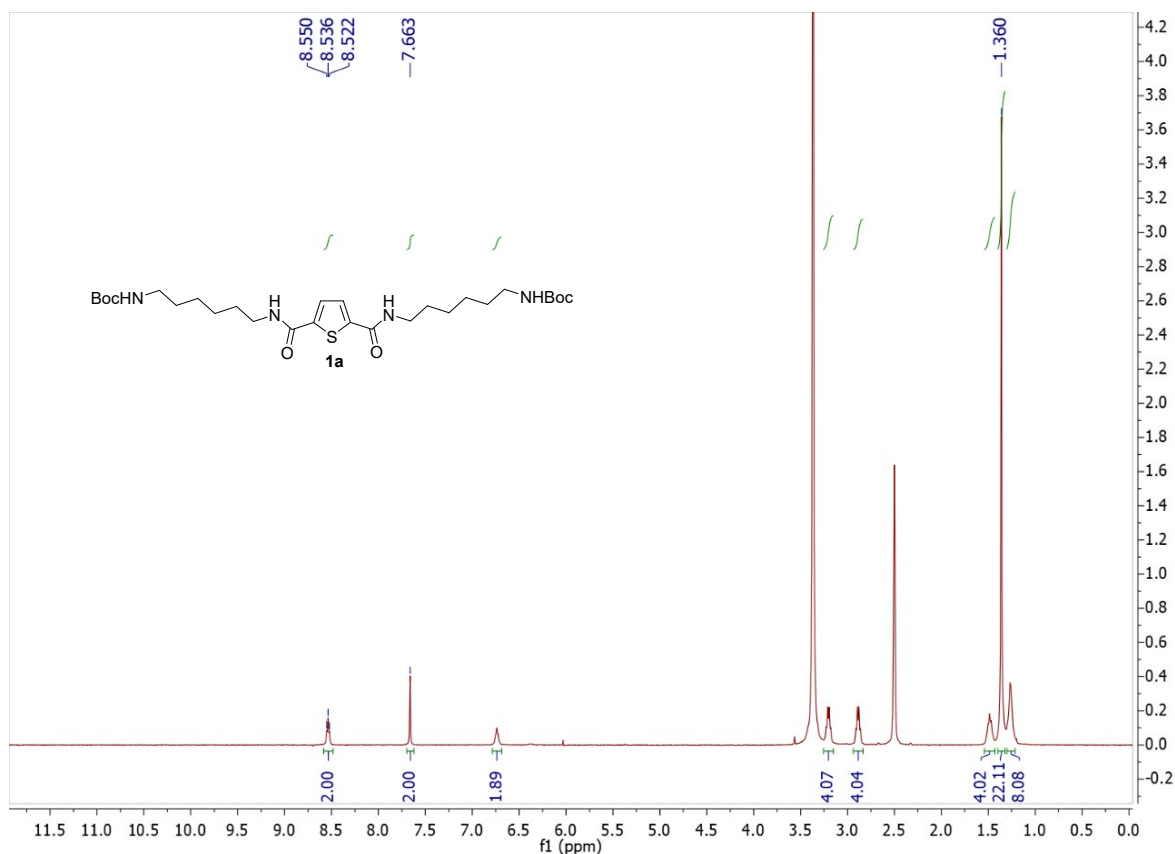


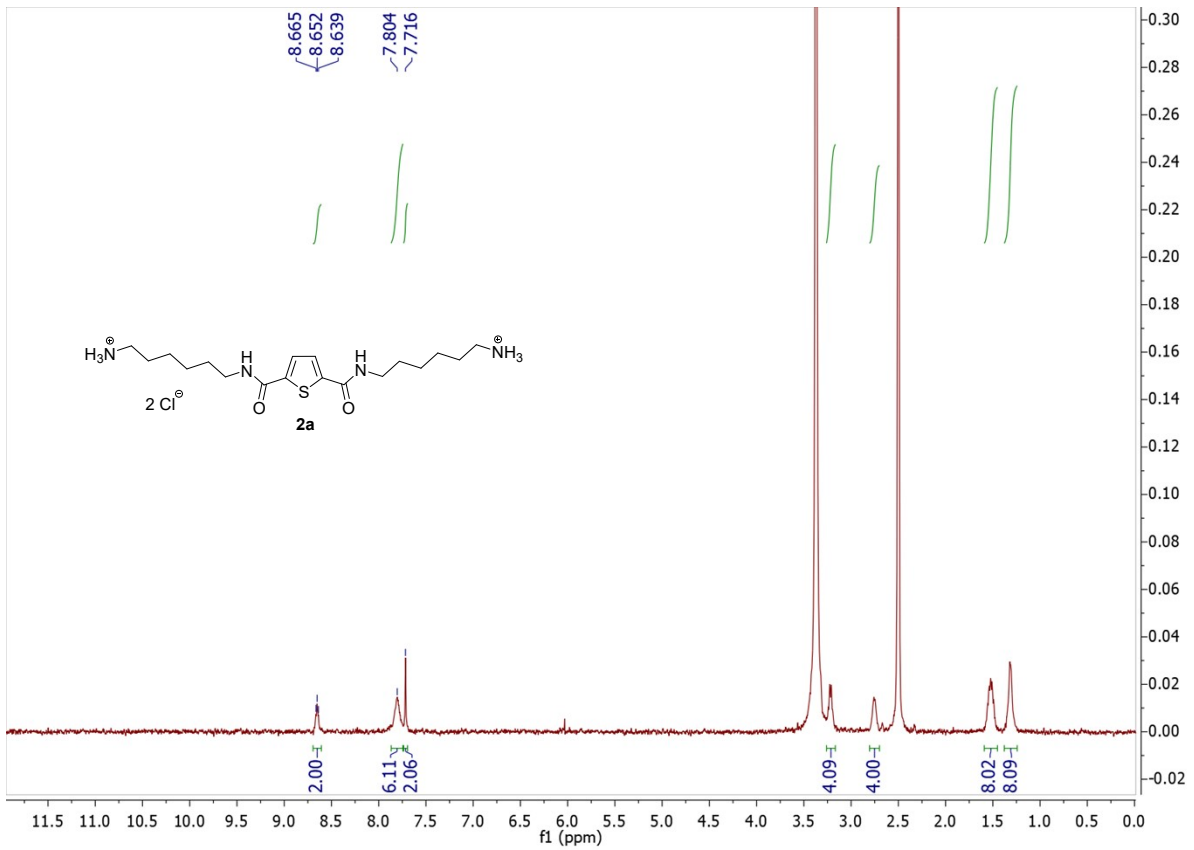
Supplementary Figure S22. Formation of the complex between **EG** with RNA over 700 ns. Color code: guanine in green, adenine in white, cytosine in grey and uracil in pink. The AO moieties of the dye are orange and the linker between them is purple.



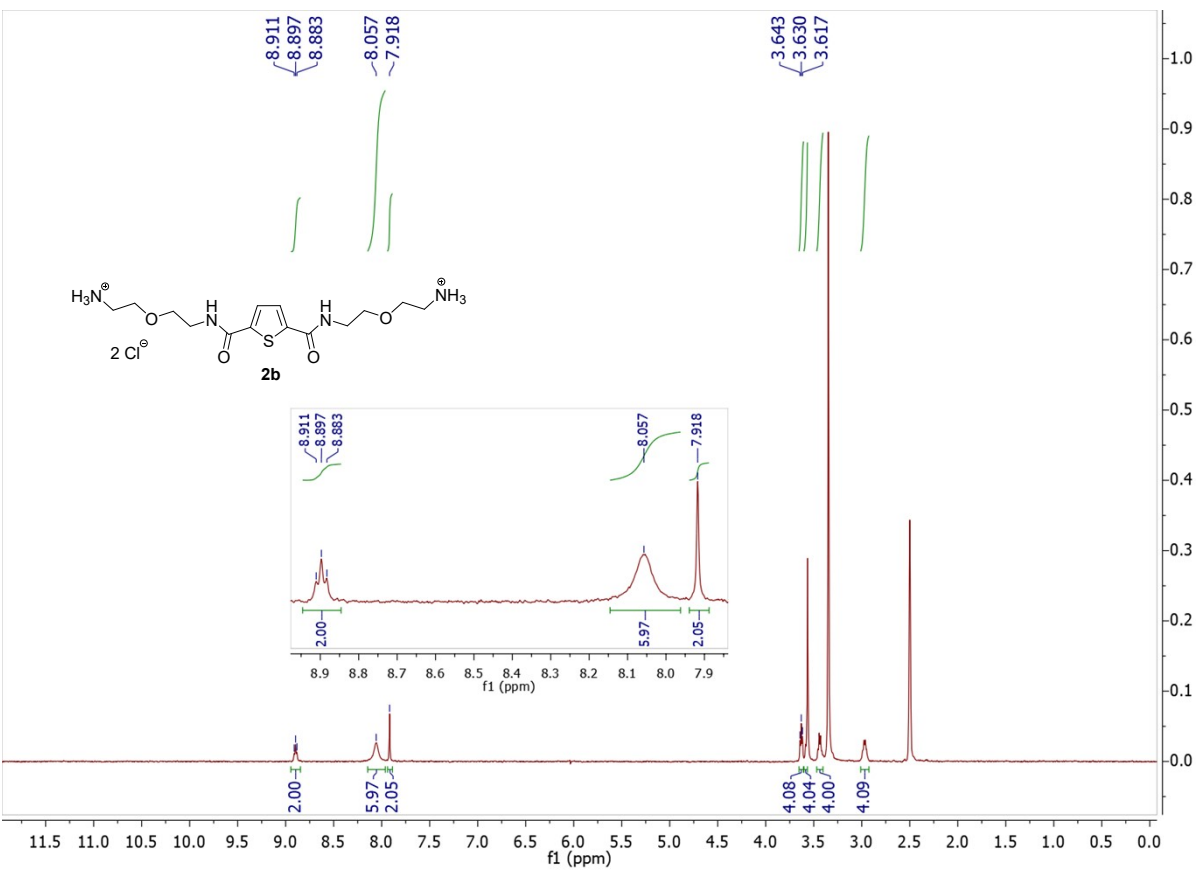
Supplementary Figure S23. Detail depicting the interaction between the thiophene moiety and a nucleic base pair, with the distance between the two highlighted (in Å).

S6. ¹H NMR spectra of the obtained compounds

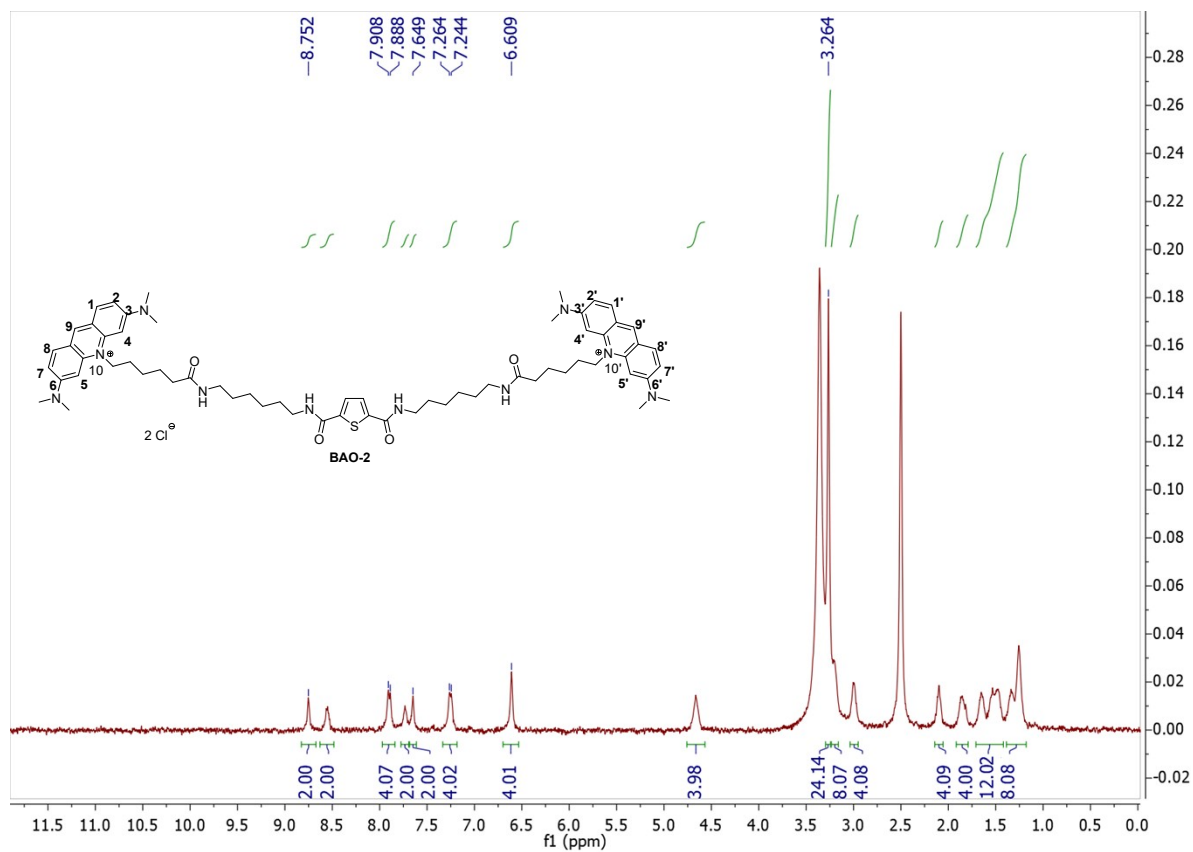




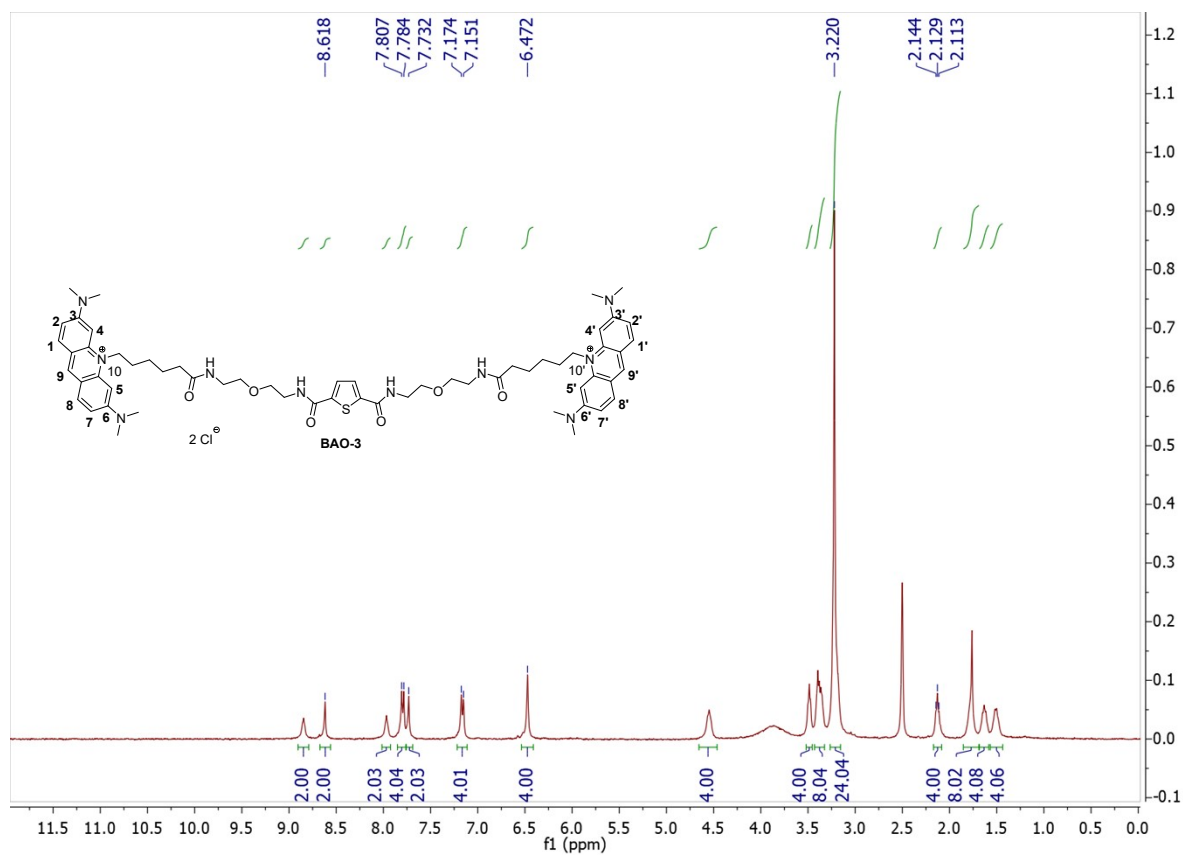
Supplementary Figure S26. ¹H NMR spectrum of **2a** (400 MHz, DMSO-*d*₆).



Supplementary Figure S27. ¹H NMR spectrum of **2b** (400 MHz, DMSO-*d*₆).

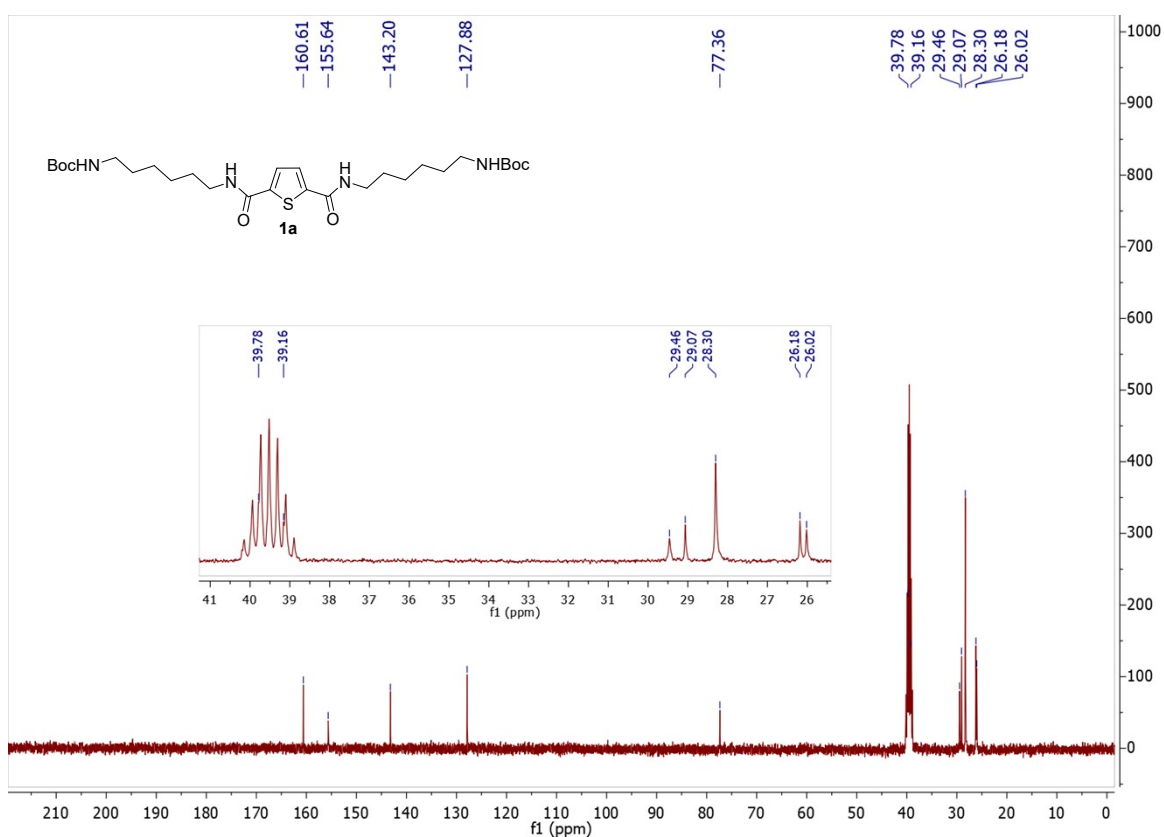


Supplementary Figure S28. ^1H NMR spectrum of BAO-2 (400 MHz, $\text{DMSO-}d_6$).

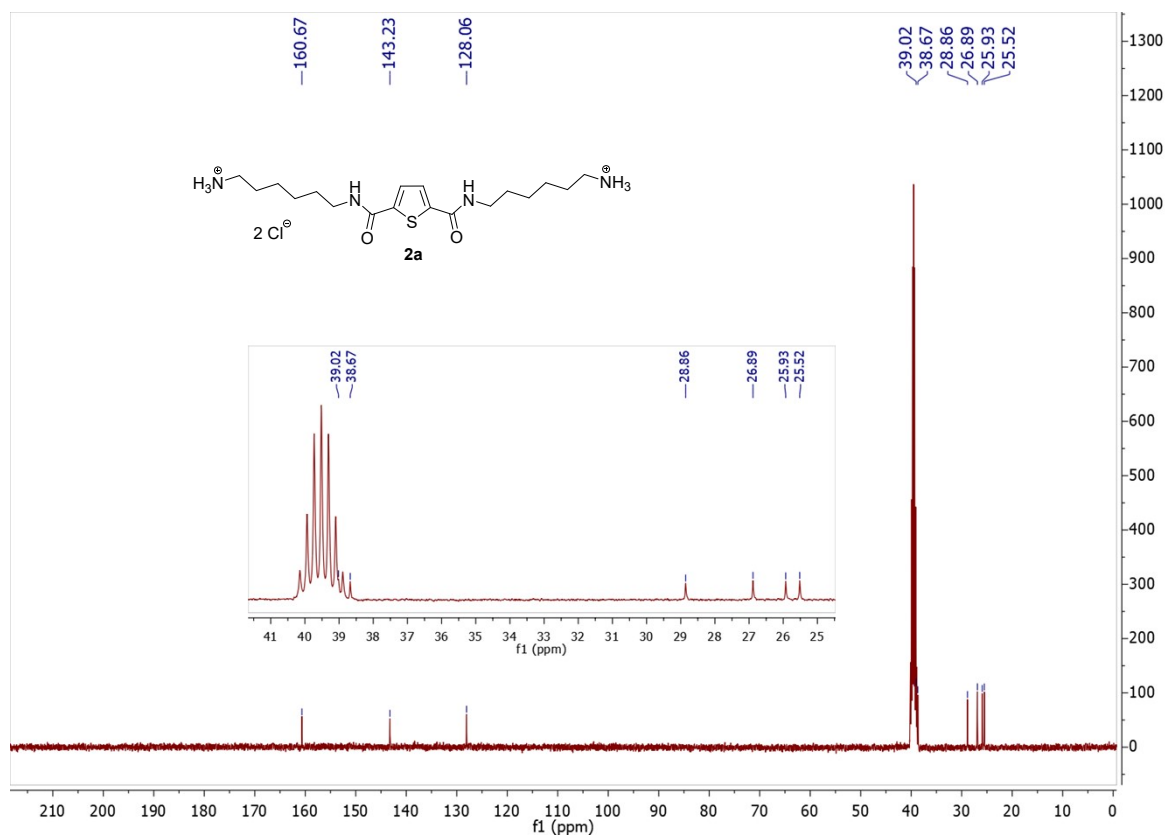


Supplementary Figure S29. ^1H NMR spectrum of BAO-3 (400 MHz, $\text{DMSO-}d_6$).

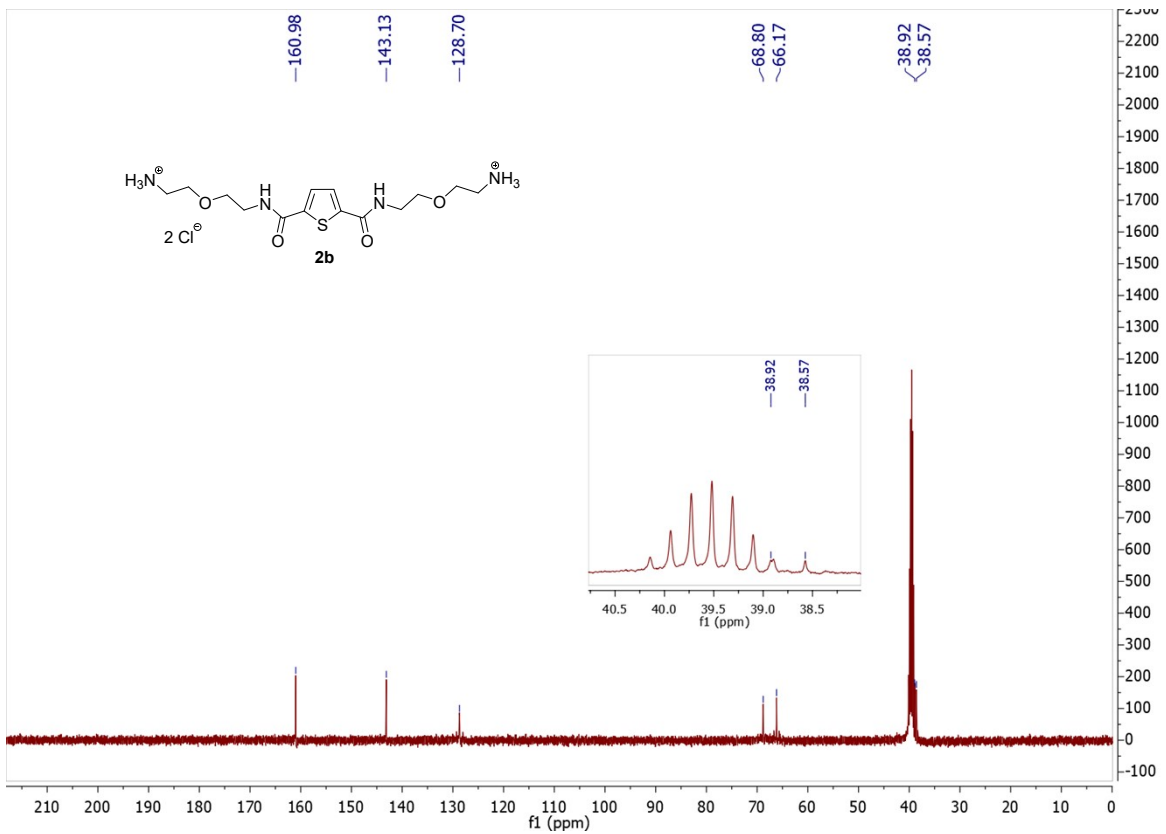
S7. ^{13}C NMR spectra of the obtained compounds



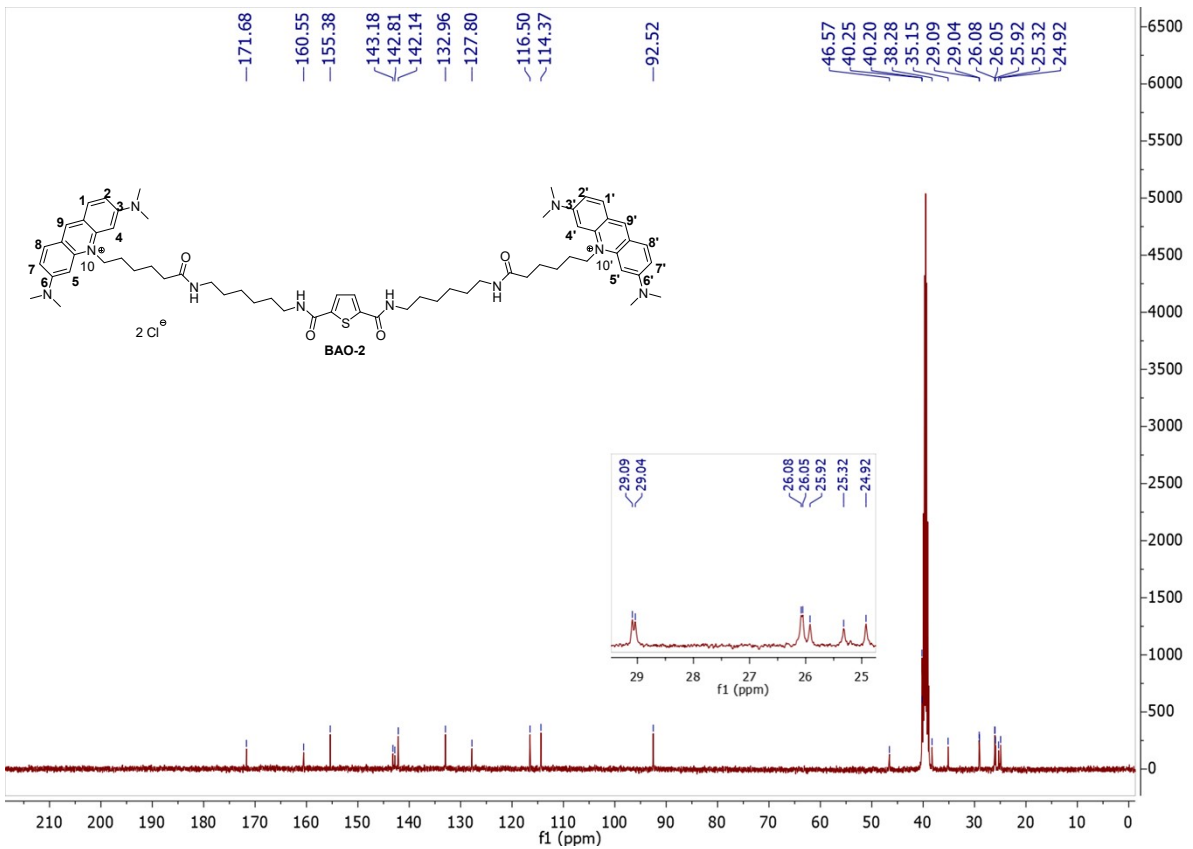
Supplementary Figure S30. ^{13}C NMR spectrum of **1a** (101 MHz, $\text{DMSO-}d_6$).



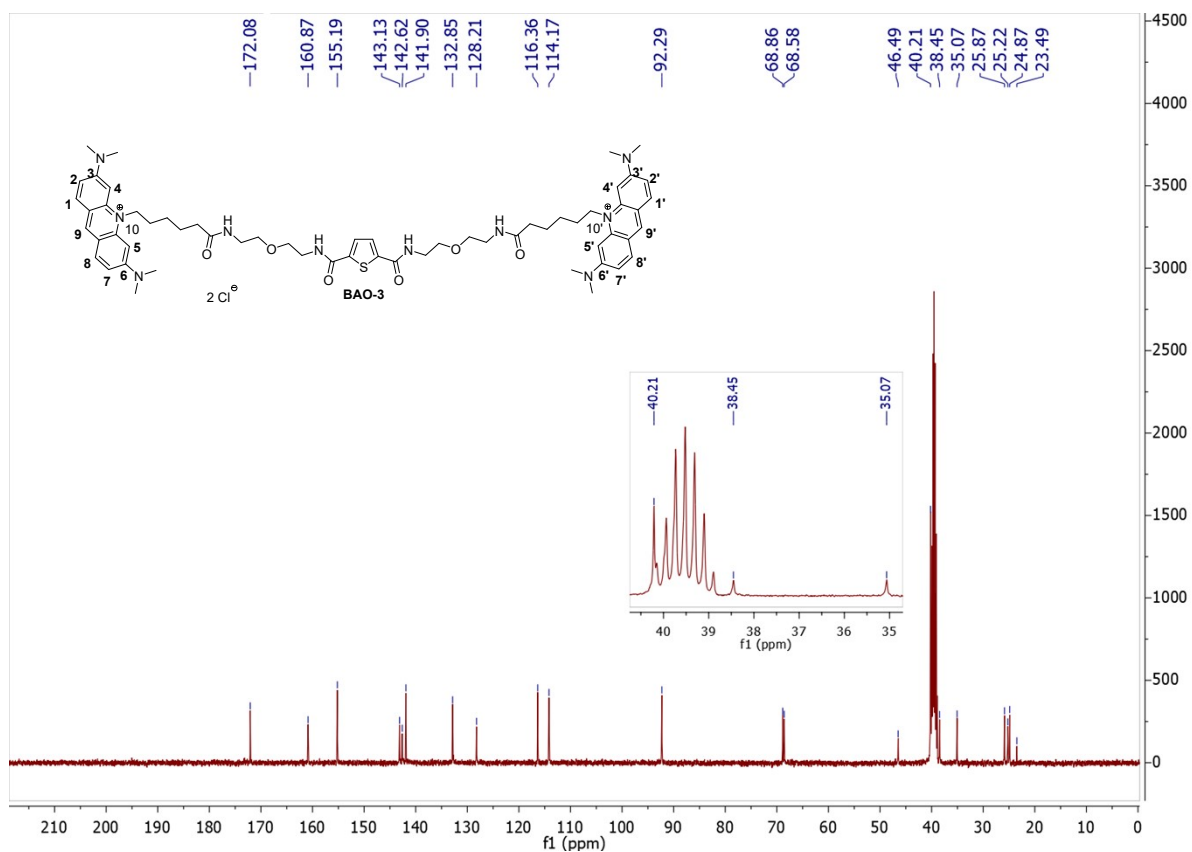
Supplementary Figure S31. ^{13}C NMR spectrum of **2a** (101 MHz, $\text{DMSO-}d_6$).



Supplementary Figure S32. ^{13}C NMR spectrum of **2b** (101 MHz, $\text{DMSO-}d_6$).

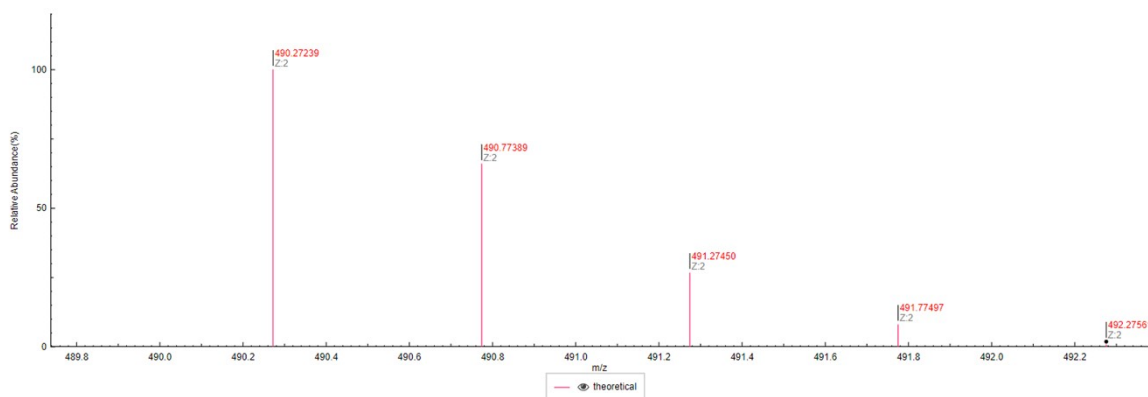


Supplementary Figure S33. ^{13}C NMR spectrum of **BAO-2** (101 MHz, $\text{DMSO-}d_6$).



Supplementary Figure S34. ¹³C NMR spectrum of BAO-3 (101 MHz, DMSO-*d*₆).

S8. HRMS spectra of the BAO dyes



D:\Data2\Rueping\ru-bao-1_240722131741

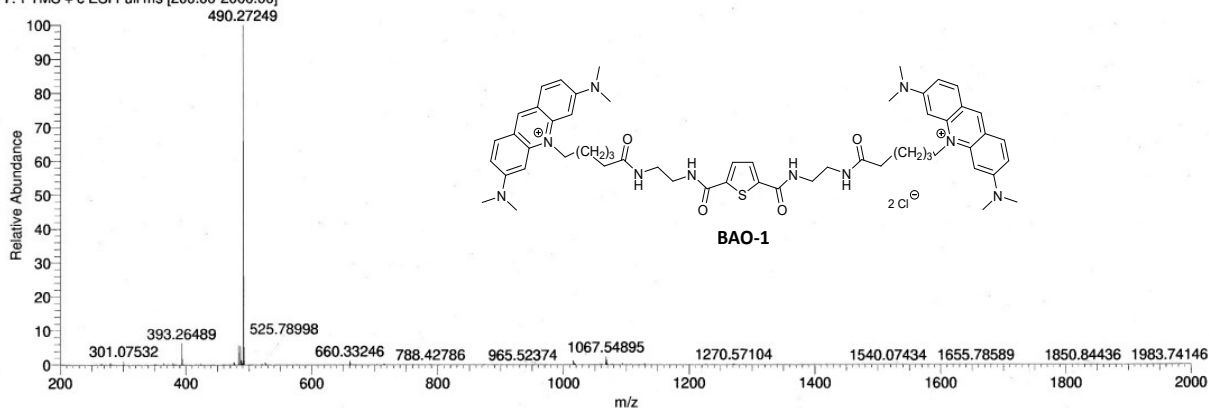
7/23/2024 9:49:13 AM

Banala\BAO-1

gel. in MeOH

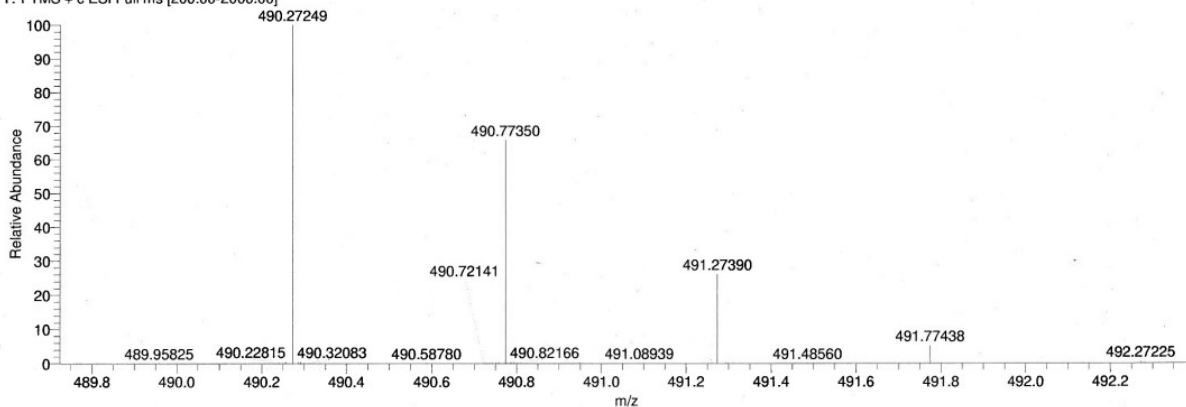
ru-bao-1_240722131741 #23 RT: 0.34 AV: 1 NL: 1.85E8

T: FTMS + c ESI Full ms [200.00-2000.00]

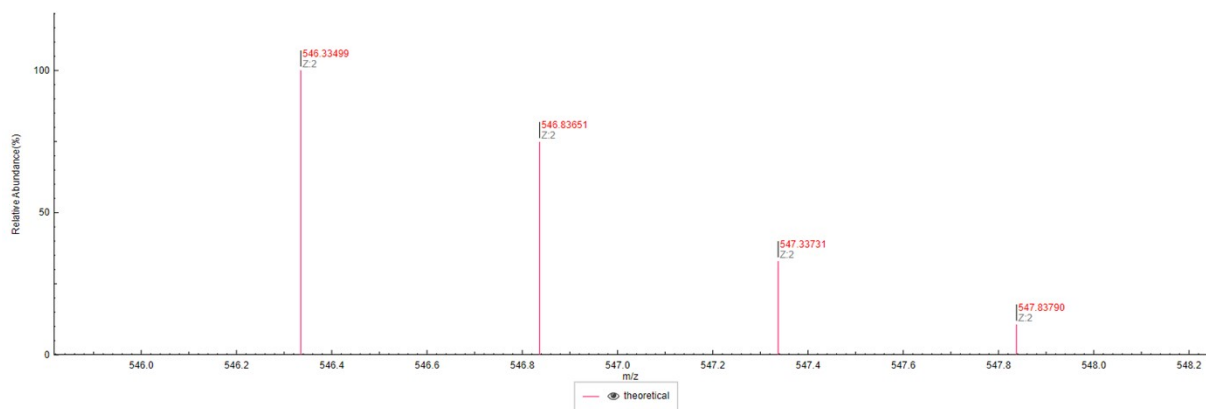


ru-bao-1_240722131741 #23 RT: 0.34 AV: 1 NL: 1.85E8

T: FTMS + c ESI Full ms [200.00-2000.00]



Supplementary Figure S35. Theoretical (in the top) and experimental HRMS spectra of BAO-1.

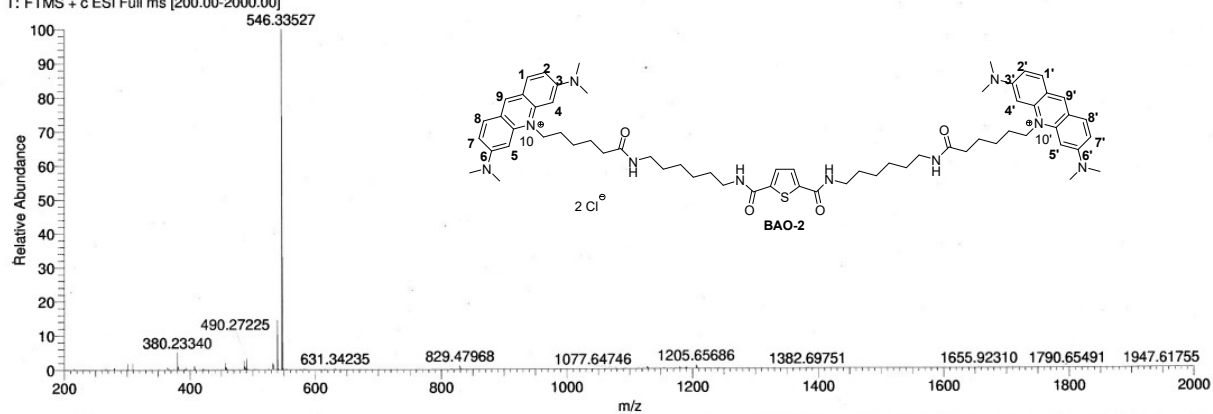


D:\Data2\Rueping\ru-bao-2_240722131741
gel. in MeOH

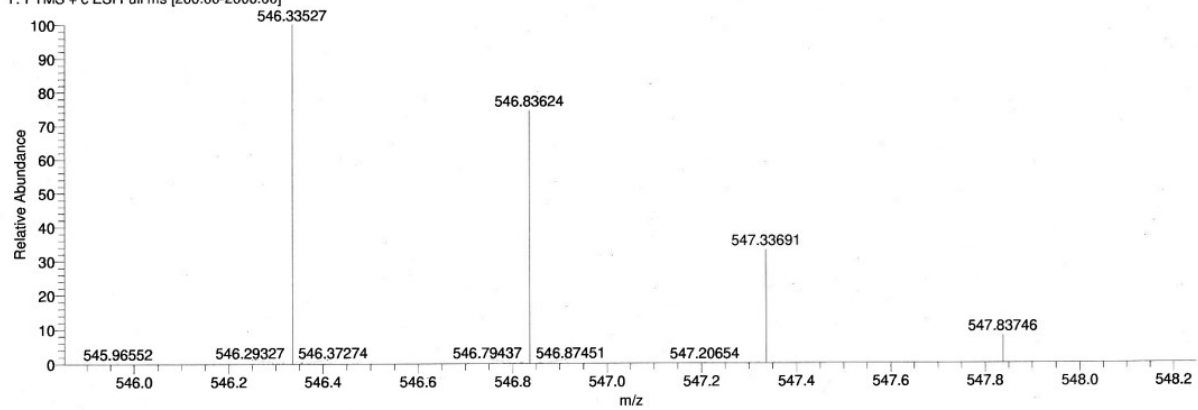
7/23/2024 9:54:47 AM

Banala\BAO-2

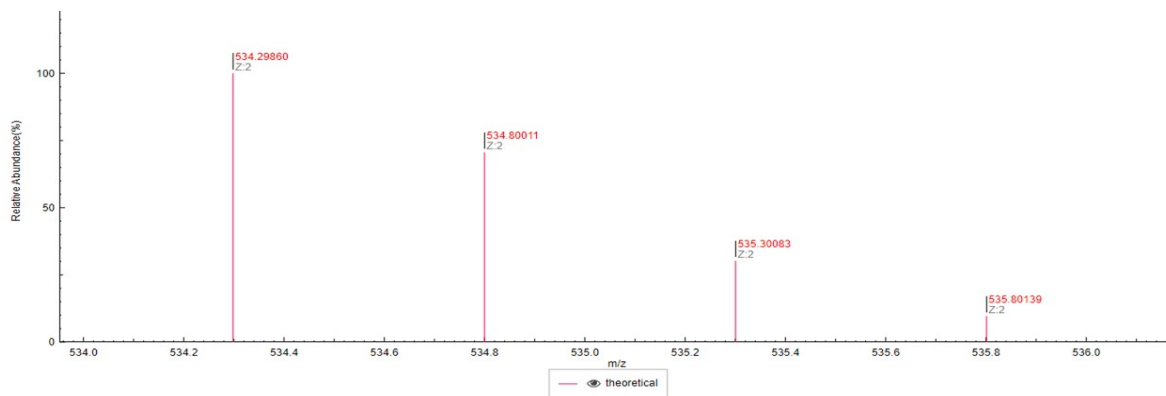
ru-bao-2_240722131741 #23 RT: 0.35 AV: 1 NL: 1.17E8
T: FTMS + c ESI Full ms [200.00-2000.00]



ru-bao-2_240722131741 #23 RT: 0.35 AV: 1 NL: 1.17E8
T: FTMS + c ESI Full ms [200.00-2000.00]



Supplementary Figure S36. Theoretical (in the top) and experimental HRMS spectra of **BAO-2**.



D:\Data2\Rueping\ru-bao-3_240722131741

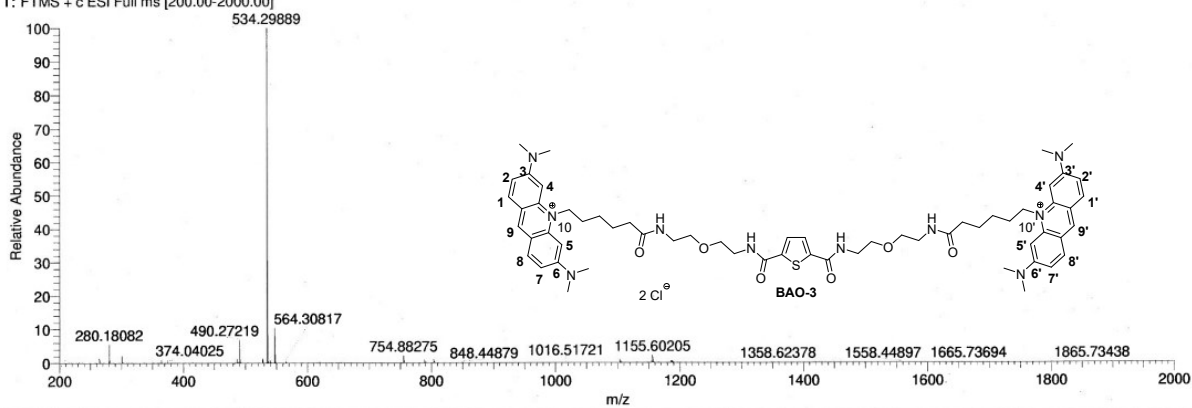
7/23/2024 9:59:23 AM

Banala\BAO-3

gel. in MeOH

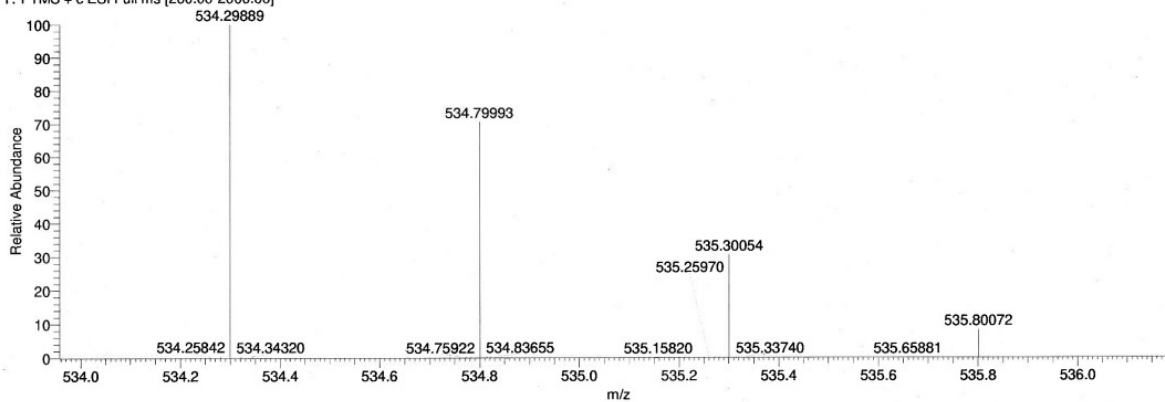
ru-bao-3_240722131741 #22 RT: 0.35 AV: 1 NL: 5.85E7

T: FTMS + c ESI Full ms [200.00-2000.00]



ru-bao-3_240722131741 #22 RT: 0.35 AV: 1 NL: 5.85E7

T: FTMS + c ESI Full ms [200.00-2000.00]



Supplementary Figure S37. Theoretical (in the top) and experimental HRMS spectra of BAO-3

References

1. O. G. Kulyk, O. S. Kolosova, R. P. Svoiakov, D. V. Kobzev, I. V. Hovor, I. M. Kraievska, E. V. Sanin, A. I. Krivoshey, Z. Y. Tkachuk and A. L. Tatarets, *Dyes Pigm.*, 2022, **200**, 110148.
2. E. Valeur and M. Bradley, *Chem. Soc. Rev.*, 2009, **38** (2), 606–631.
3. H. E. Gottlieb, V. Kotlyar and A. Nudelman, *J. Org. Chem.*, 1997, **62** (21), 7512–7515.
4. Y. Kubota and R. F. Steiner, *Biophys. Chem.*, 1977, **6**, 279–289.
5. M. Hammer, D. Schweitzer, S. Richter and E. Königsdörffer, *Physiol Meas.*, 2005, **26** (4), N9-12.
6. D. Magde, G. E. Rojas and P. G. Seybold, *Photochem. Photobiol.*, 1999, **70**, 737-744.
7. J. R. Lakowicz, *Principles of fluorescence spectroscopy*. 3rd ed. Springer; 2006.
8. P. Schmidpeter and C. Nimigean, *Bio Protoc.*, 2018, **8**, e3041.
9. J. S. Lolkema and D.-J. Slotboom, *J. Gen. Physiol.*, 2015, **145**, 565–574.
10. E. N. de Boer, P. E. van der Wouden, L. F. Johansson, C. C. van Diemen and H. J. Haisma, *Gene Ther.*, 2019, **26**, 338–346.
11. P. Kumar, A. Nagarajan and P. D. Uchil, *Cold Spring Harb. Protoc.*, 2018, **6**, 469–471.
12. M. Berridge, P. M. Herst and A. S. Tan, *Biotechnol. Annu. Rev.*, 2005, **11**, 127–152.